Chapter 1

# Introduction

# A brief review on Raman and Surface Enhanced Raman Spectroscopy

# Introduction:
# A brief review
# on Raman and
# Surface Enhanced Raman Spectroscopy

## 1.1 Introduction

Surface Enhanced Raman Spectroscopy (SERS) is the phenomenon of gigantic enhancement of Raman signal by molecules adsorbed on different metal substrates.

Raman signal can be used as a fingerprint for a given structure of molecule as different structure exhibits characteristic Raman spectra.

However, detection by this method requires highly sensitive and optimized arrangement. Fluorescence of the impurities of the given sample can affect the Raman spectra and the given sample of study could be modified by the heat of the laser radiation. The output radiation of a particular Raman spectrum is very weak in nature.

In SERS, the enhancement factor increases up to $10^{10}$ to $10^{11}$ times the Normal Raman Spectroscopy. Thus SERS can be used as a powerful spectroscopic technique which overcomes the weak scattering cross-section of normal Raman spectroscopy [1, 2].

In this chapter, the mechanisms involved in Raman scattering as well as in the enormous enhancement of Raman signal of the molecules adsorbed on suitable metal surfaces are discussed.

## 1.2 Raman spectroscopy

Raman spectroscopy is a useful vibrational spectroscopic technique which can provide information on molecular vibrations and crystal structures. Light is scattered by a matter when incident on it.

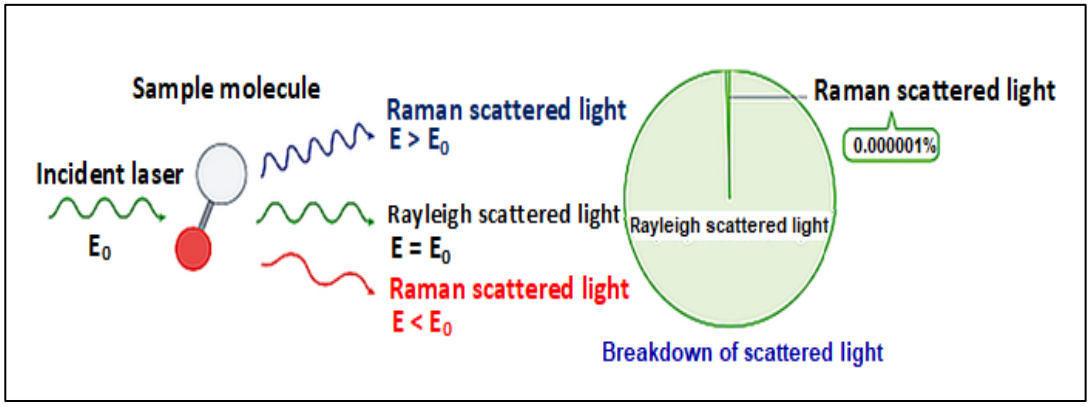


**Figure 1.1:** Elastic and inelastic scattering of light

Although almost all of the scattering is an elastic process, there is a very small percentage of scattering which is an inelastic process. In elastic scattering, known as Rayleigh scattering, the scattered light does not undergo a change in frequency. On the other hand a scattered light has different energy from incident light in inelastic process. This inelastic scattering of light was proposed theoretically by Smekal in 1923 [3] and first observed experimentally by **Sir Chandrasekhara Venkata Raman** and K.S. Krishnan in 1928 [4]. This is known as Raman scattering and for this discovery, professor C.V. Raman was awarded with prestigious Nobel Prize in the year 1930.

## 1.2.1 Stokes and anti-Stokes lines

The spectrum of scattered light consists of lines of same frequency as that of the incident beam, known as, *Rayleigh lines* and in addition, certain week lines of changed frequencies called *Raman lines*. The Raman lines are symmetrically present on the two sides of the Rayleigh lines. The lines on low frequency side are called Stokes lines and those on high frequency side are *Anti-stokes lines*.

Although the effect was strong as it was measured by Sir Raman from concentrated pure organic solvents and visible to human eyes, the effect has been very week for comparatively less concentrated solutions of solids. The demerits have been overcome by discovery of efficient detection systems like, holographic gratings, photomultipliers, coupled devices, notch filter etc. Intense monochromatic lasers are being used as the incident light.

Oscillating polarization is produced in the molecules by the photons coming from the laser radiation of high intensity and a "virtual state" is formed. This polarization may couple with the other possible polarizations as well as with the vibrational and electronic excitations. In absence of such coupling the vibrational state of the molecule remains unchanged and elastic Rayleigh scattering occurs.

However, if the oscillating polarization couples with vibrational state such that a molecule is excited from the ground level and falls to a vibrational level which is higher in energy than the state it started in, the scattered photon will of energy less than that of the incident photon. These photons are called *Stokes scattered photons* and the corresponding lines are called *Stokes lines*. On the other hand, photons of energy higher than that of the incident photon are scattered when the molecule is excited from the higher vibrational state and falls to the ground state. These photons and are called *anti-Stokes scattered photons* and the corresponding lines are called *anti-Stokes lines* [5]. Figure 1.2 illustrates the origin of Rayleigh lines, Stokes Raman lines and Anti-Stokes Raman lines.

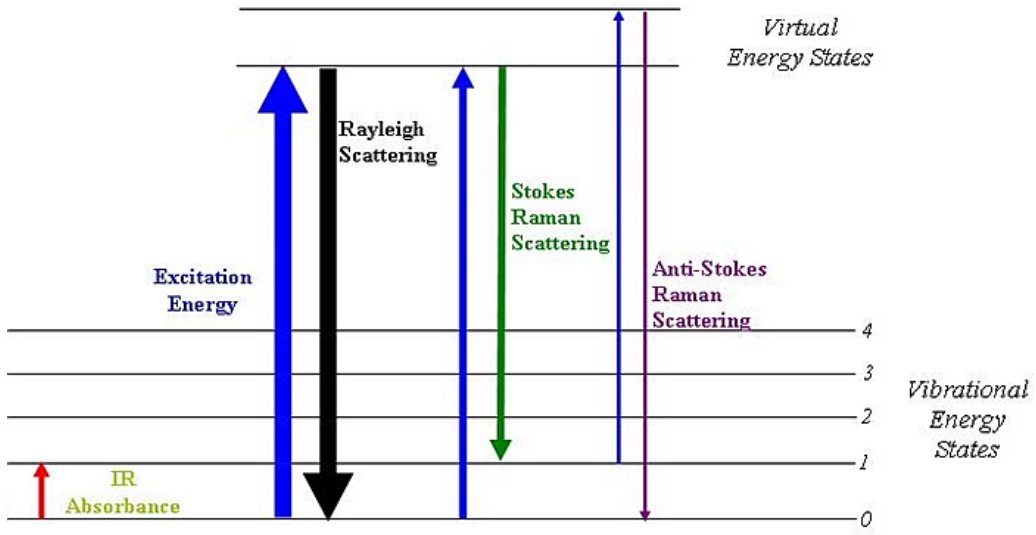


**Figure 1.2:** Schematic diagram: Rayleigh, Stokes Raman and Anti-Stokes Raman scattering

The anti-Stokes lines originate from the molecule initially in a vibrationally excited state. Population of such molecule is much less, in room temperature, than that of molecules in the ground sate. As a result the anti-Stokes lines are typically much less intense. Conversely, Stokes lines are brighter than anti-Stokes lines simply because there are more molecules in the ground state.

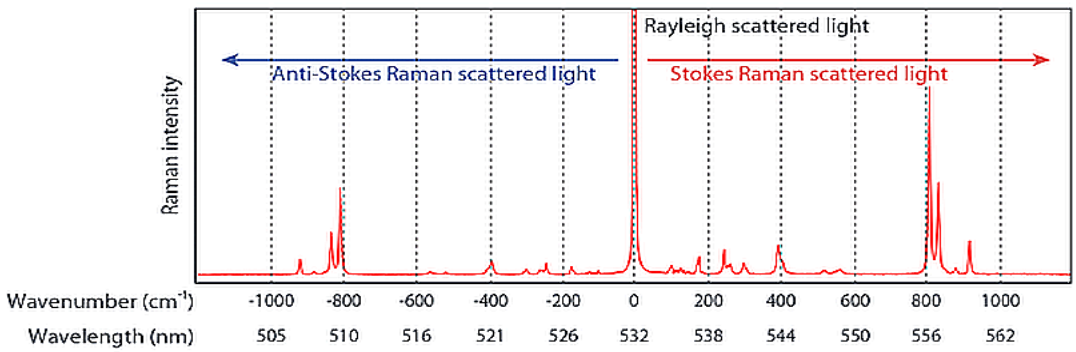


**Figure 1.3:** Stokes and anti-Stokes lines of ethanol (excitation wavelength =532 nm)

The symmetrical distribution of anti-stokes and stokes line from the Rayleigh line implies that in both the processes the scattered photons have same amount of

energy gain or loss which implies that both the anti-Stokes and Stokes lines originate from the same virtual level.

## 1.2.2 Raman selection rules

Raman spectroscopy provides information about a molecule's composition, vibrations and rotations. Vibrational information of a molecule can also be obtained from infrared (IR) absorption spectroscopy measuring the interaction of the infrared light and the chemical species of interest. In fact Raman and IR spectroscopy are two main spectroscopic tools complementary to each other in the detection of the vibrations in a molecule.

The selection rule of IR spectroscopy is that there must be a net change in permanent dipole moment during the vibrations. On the other hand, a vibration is Raman-active, when the polarizability of the molecule changes with the vibrational motion.

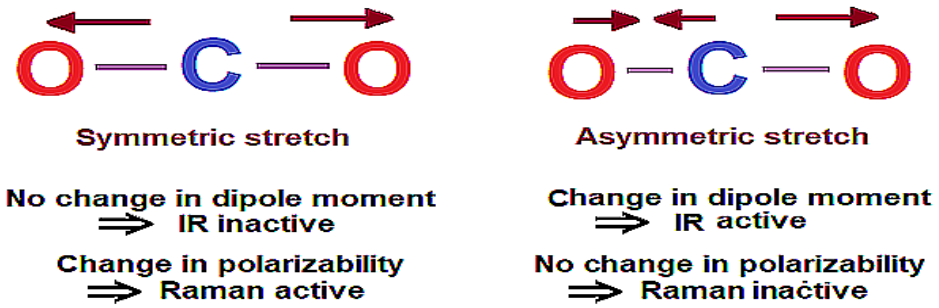


**Figure 1.4:** Illustration on Raman active and IR active vibration

As shown in Figure 1.4, the symmetric stretch in carbon dioxide does not result in change of dipole moment and thus it is not IR-active. The asymmetric stretch is IR-active as there is a change in dipole moment due to this vibration.

The symmetric stretch in carbon dioxide leads to change in molecular polarizability and it is demonstrated in Figure 1.5. The shape of electron cloud in the equilibrium state is different from that when it is in the extended and compressed symmetric motions. The symmetric stretch is, therefore, Raman-active.

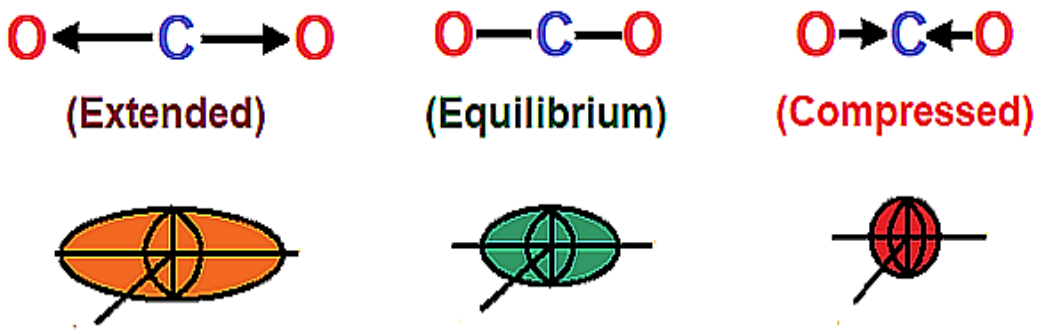


**Figure 1.5:** Change of polarizability in symmetric stretch

Whereas IR bands arise from a change in the dipole moment, Raman bands arise from a change in the polarizability. In many cases, transitions that are allowed in Raman are forbidden in IR, so these techniques are often complementary.

## 1.2.3 Theory of Raman scattering

Although the first experimental evidence for the inelastic scattering of light by molecules such as liquids was observed by Raman and Krishnan in 1928, the Raman effect was first theoretically predicted by Smekal in1923; followed by quantum mechanical descriptions by Kramers and Heisenberg in1925 and Dirac in 1927.

### 1.2.3.1 Classical theory

According to the classical theory [6], the incident electromagnet field induces an electric dipole moment on the scattering system (molecule or solid). Such an

induced dipole moment is oscillating with the frequency of the incident radiation and is acting as a secondary source for electromagnetic radiation. Here, the molecules are considered to execute simple harmonics vibrations and the quantization of the rotational and vibrational energy levels are not taken into account.

The oscillating electric field of the incident light results in separation of positive and negative charge centers and thereby induces dipole in the molecule with or without exchanging energy with vibrations in the molecules.

If μ be the induced dipole and E be applied electric field then we may write

$$\mu = \alpha E \tag{1.1}$$

where, $\alpha$ is the polarizability of the molecule

The time-dependent electric field may be taken as $E = E_0 \cos 2\pi\nu t$, where ν is the frequency of the incident light.

Then,

$$\mu = \alpha E = E_0 \cos 2\pi\nu t \tag{1.2}$$

Due to some internal motion of the molecules such as vibration rotation, the polarizability changes periodically. These vibrations will be then superimposed on the oscillating dipole.

If $\nu_{vib}$ is the internal vibrational frequency then we may write,

$$\alpha = \alpha_0 + \beta \sin 2\pi\nu_{vib} t \tag{1.3}$$

as $\alpha$ changes with $\nu_{vib}$.

Now, after considering the internal motions of the molecules, the electric dipole will have the value

$$\mu = \alpha E = (\alpha_0 + \beta \sin 2\pi\nu_{vib} t)\, E_0 \cos 2\pi\nu t$$

$$=\alpha_0 E_0 \sin 2\pi\nu t + \frac{1}{2}\beta E_0 \{\cos 2\pi(\nu - \nu_{vib})t - cos\, 2\pi(\nu + \nu_{vib})t\} \quad (1.4)$$

The first term in the equation (1.4) represents the Rayleigh scattering and the second term represents the Raman scattering. In Raman scattering, the high frequency term is called anti-Stokes shift and the low frequency term is called Stokes shift.

It may be noted that, if $\beta$ is equal to zero, the second term will be vanished. Therefore, Raman scattering will be observed if the molecular vibration or rotation (or both) changes the polarizability of the molecule.

### 1.2.3.2 Quantum theory

According to quantum theory, Raman scattering is a process which involves instantaneous absorption of an incident photon and subsequent emission of another photon. The emitted photon is inelastically scattered by the molecule and emitted with different frequency as compared to absorbed photon.

During the scattering process the molecule may move either to a more vibrationally excited state of the ground electronic state or to a less vibrationally excited state. In the former case, the photon is emitted with energy lowered by an amount equal to a vibrational transition and are called Stokes scattered photons. In the latter case, the emitted photon is of energy higher than that of the incident photon and termed as anti-Stokes scattered photons.

If $\nu$ and $\nu'$ are incident and scattered frequencies and E and E′ are the initial and final molecular energy levels then, from the energy conservation law, we may write

$$h\nu + E = h\nu' + E' \quad (1.5)$$

$$\Delta E = h(\nu - \nu') \quad (1.6)$$

Now, from the theory of Raman scattering, the elastic and inelastic scattering can be expressed as,

(1) Rayleigh lines, ΔE=0, when $\nu = \nu'$

(2) Stokes lines, ΔE<0, when $\nu > \nu'$

(3) Anti-Stokes lines, ΔE>0, when $\nu < \nu'$

In Raman experiments, the Raman shift is measured in wave number and it is given by

Raman shift, $\Delta\lambda(\text{cm}^{-1}) = (\frac{1}{\lambda 0} - \frac{1}{\lambda 1})$

where, $\lambda_0$ is the excitation wavelength and $\lambda_1$ is the Raman scattered wavelength in cm.

### 1.2.3.3 Raman scattering cross-section

Raman scattering cross section σ (say) gives a measure of the efficiency of the Raman scattering process and it is the fraction of the incident power that is inelastically scattered by the molecules concerned. Thus, the power scattered by the molecules for an incident power $S_0$ is given by,

$$P = \sigma S_0 \tag{1.7}$$

This power P is scattered in all possible directions and the spectrometer collects a part of it as it is set in a specific direction. Thus, the measured Raman intensity is actually that corresponding to the differential Raman cross section dσ/dΩ given by,

$$\langle I_R \rangle = (\frac{d\sigma}{d\Omega}) S_0 \, d\Omega \tag{1.8}$$

where, So is incident laser intensity at molecular position and dΩ is the small solid angle subtended by the collecting optics at the molecular position. Here, $\langle I_R \rangle$, the Raman scattered intensity, is the average of the signal obtained for a given vibrational mode of a single molecule over all orientations [7, 8]

From the above equation the total Raman scattering cross-section can be obtained as

$$\sigma = \int \left(\frac{d\sigma}{d\Omega}\right) d\Omega \qquad (1.9)$$

### 1.2.3.4 Intensity of Raman line

Intensity of Raman scattered photons $I_R$ is proportional to the dipole moment induced ($P_{ind}$) in the molecule by the electric field $\mathbf{E_0}$ of the incident light. The molecular polarizability $\boldsymbol{\alpha}$ is the responsiveness of the molecule to the incident electric field in respect of induction of dipole moment in it.

In terms of the molecular polarizability tensor and the electric field intensity, the Raman intensity can be expressed as

$$I_R = \left|P_{ind}\right|^2 \propto \left|\vec{\alpha}\vec{E}_0\right|^2 \qquad (1.10)$$

Incident photon transfer energy in Raman spectra unveil the energy transfer between the photons and molecules during their interaction. Hence a molecule exhibits Raman scattering only if there is a change in the molecular polarization potential or deformation of the electron cloud with respect to the vibrational coordinates [9].

## 1.3 Advantages and limitations of normal Raman spectroscopy

There are certain advantages and limitations of normal Raman spectroscopy as described below:

## 1.3.1 Advantages of Raman spectroscopy

- Raman spectroscopy can give information in respect of many organic and inorganic materials in the form of solids, liquids, polymers or vapours.
- Sample preparation is usually simple.
- As the spectral measurements on vibrations made in the visible region, glass cells may be used
- Raman spectra are highly specific like a chemical fingerprint of a material.
- Raman spectra are obtained with very short exposure (within seconds).
- The intensity of the Raman lines is related to the number of molecules in the sample and can be used for quantitative analysis
- Very small volume of the sample is required for recording Raman spectra.

## 1.3.2 Limitations of Raman spectroscopy

- As the Raman signal is very weak, the detection needs a sensitive and highly optimized instrumentation [10].
- Sometimes the Raman spectra of a sample remain hidden in the fluorescence of impurities.
- Intese laser radiation required for obtaining Raman spectra may sometime destroy the sample.

In order to overcome the drawbacks of Raman scattering process, several new techniques are introduced. SERS is one of the most significant methods used to reduce the drawbacks of normal Raman spectroscopy.

# 1.4 Surface Enhanced Raman Spectroscopy (SERS)

## 1.4.1 Discovery of SERS

In 1974, the group Fleischmann, Hendra and McQuillan [1] observed intense Raman scattering from pyridine adsorbed on the roughened silver electrode. Their initial idea was to produce a large surface area on the roughened surface for developing a spectroscopic probe by which electrochemical process could be studied. They applied about 450 potential oxidation and reduction cycles (ORC) to an Ag electrode in an aqueous electrolyte comprised of 0.1mol l–1 KCl + 0.05 mol l–1 pyridine. The output spectrum was found to be of surprisingly high quality which varies with the electrode potential. They initially explained that the large enhancement might have taken place due to the increasing number of scatterers present in the enhanced surface area.

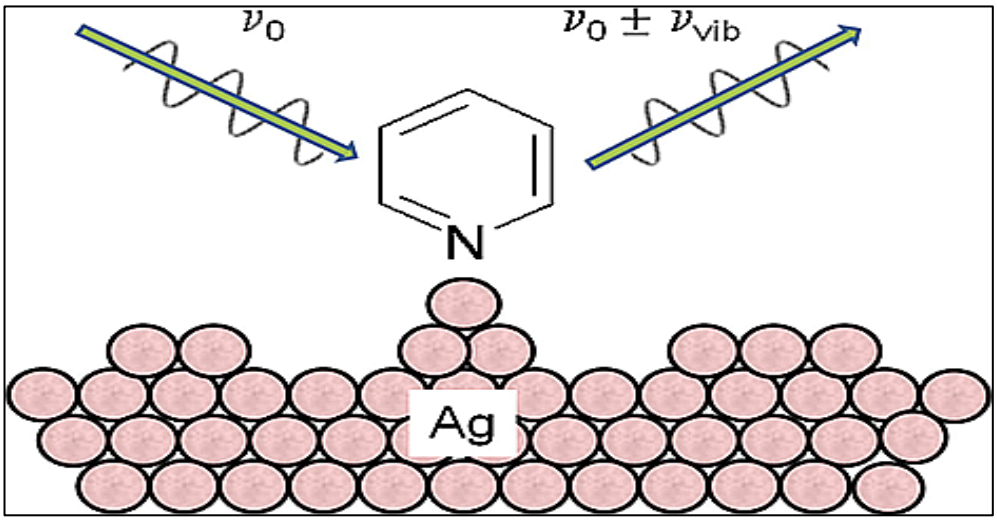


**Figure 1.6:** A schematic representation of SERS with pyridine adsorbed on silver

Later in 1977, Jeanmaire and Van Duyne [11] and Albrecht and Creighton [12] independently recognized that the large enhancement was not due to the increased surface area and the two groups then provided strong evidences that an enhancement of the scattered intensity occurred in the adsorbed state. This large enhancement effect has been named as **Surface Enhanced Raman Spectroscopy (SERS)**. The exact mechanism behind the large enhancement is still not completely known and further research is being carried out. However, the reason behind the large enhancement of the weak Raman signal is being supported by two main mechanisms. Jeanmaire and Van Duyne tentatively proposed the electromagnetic field enhancement mechanism and on the other hand Albrecht and Creighton speculated the chemical enhancement mechanism. Whereas localized surface plasmon is the main reason behind the electromagnetic field enhancement mechanism, the chemical enhancement mechanism is based on the charge transfer effect between the adsorbed molecule and metal surface.

Since discovery by Fleischman et al. [1] SERS has been developing over last four and half decades [13-15] and in recent days it has become a versatile analytical technique [16].

After more than 40 years of research on SERS and over 10,000 publications a universal agreement now exists regarding the origin of SERS. Mainly two types of mechanisms contribute to the effect: (i) electromagnetic effects (EE) that involves localized surface plasmon resonance and (ii) chemical effect (CE) arising from electronic interaction between the adsorbed molecule and nano structured metal surface [17].

When illuminated with light of such wavelength that can excite surface plasmon, the electromagnetic energy is concentrated. The appropriate nano surface, then, acts as receiving as well as radiating antenna simultaneously. Both the incident and the Raman scattered lights are, thus, enhanced and result in massive signal enhancement achieved in SERS which can now detect a single molecule [18].

Chemical effect is proposed as supplementary to the plasmonic theory as the later cannot fully explain the SER spectra alone. Chemisorption of a molecule on a metal is thought to be due to metal-ligand complex formation [18], metal to molecule or molecule to metal charge transfer [19, 20], radial ad-molecule anion formation by the hot electron metal transiently residing on the ad-molecule [21]. SERS enhancement is in excellent agreement with the predictions for various metals on the basis of the strength and quality factor of the surface plasmon and the concerned wavelength range where silver emerges to be the "enhancement champion" [22].

## 1.4.2 Key features of SERS

SERS has now become an attractive technique to detect a wide range of chemical species because of the sensitivity of SERS, as well as its exceptional spectral selectivity. These include benzene, toluene, ethylbenzene, and xylenes [23–26]; polycyclic aromatic hydrocarbons [27–230]; volatile organic compounds such as chlorinated solvents [24, 31] and methyl t-butyl ether [22]; heavy metals; toxic or radioactive cations/anions [32–40]; ionic nutrients [32, 41–43]; pesticides [44–48]; drugs and pharmaceuticals [49–54]; and explosive materials [55–59]. SERS has also been combined with other analytical techniques such as gas chromatography [60, 61], thin layer chromatography [62], liquid chromatography and flow injection analysis [63–65], and electrochemistry [66, 67].

SERS can be used for successful detection of trace amount of chemical analytes when certain requirements are satisfied [68-71] as mentioned below:

- Choice of the metal should be proper. Mainly the coinage metals, silver, gold and copper are used for SERS. The enhancement factor for these metals ranges from $10^6$ to $10^{14}$ depending on the morphology of the surface, chemical nature of the adsorbed molecules and some other factors.

- Strong SERS signal is obtained when roughness of the metal surface is ~10-200 nm with appropriate surface morphology. The roughness at atomic scale, such as certain ad-atoms, ad-clusters, steps, kinks or vacancies can assist further enhancement. Thus the surface should be suitably roughened to achieve desired morphology.

- The analyte must absorb on the surface effectively.

- Molecules adsorbed in the first layer on the surface show the largest enhancement and as the distance of the molecule from the surface increases the enhancement decreases. Thus concentration of the molecules should ensure monomolecular coverage for largest enhancement.

- Intensity of the excitation light must be such that there is no surface photochemistry.

- For quantitative measurements many events should be averaged by controlling the number of active sites.

## 1.4.3 SERS substrates

Since discovery of surface enhanced Raman spectroscopy, a large number of substrates have been prepared for this purpose. Silver, copper and gold are the leading substrates but some other substrates have also been reported [72, 73]. Although silver provides higher SERS enhancement than gold, the latter is more useful for biological and biomedical applications due to its long-term stability and biocompatibility.

SERS activity strongly depends upon the nature of the substrate. In order to obtain uniform output SERS signal, the surface of the substrate should be homogeneous. The contribution of electromagnetic field enhancement mechanism is very large in the overall enhancement of SERS spectroscopy. The reason behind the large electromagnetic enhancement is surface plasmon resonance (SPR) which is best

achieved when the imaginary part of the dielectric constant of the metal has low value. However, the value of the imaginary part of the dielectric constant is large in the visible light region [74] and the SERS factor is very low, ranging from 10 to $10^3$ for transition metal.

It is found that the activity of SERS depends upon the size, shape and aggregation of nanoparticles. Several techniques of nanoscience have been employed for the fabrication and characterization of SERS substrates. Even SERS spectra of a single molecule with a large output signal have been found by adsorbing the molecule on well characterized silver or gold nanoparticles [74].

In surface enhanced Raman spectroscopy research, the fabrication of the SERS-active substrate is very important object. The most commonly used substrates are metal colloids of coinage metals like silver, copper and gold and metal electrode surfaces roughened by one or more electrochemical oxidation reduction cycles [74].

The recent advanced technology of nanoscience has been applied to construct several SERS-active substrates, like various nano structures from nanoparticles to nano wire, nanosphere, nanorod. SERS substrates can be roughly classified into three parts: *(1) metal nanoparticles in suspension, (2) metal nanoparticles immobilized on solid substrates and (3) nanostructures fabricated directly on solid substrates, which includes nanolithography and template-based synthesis of nanostructures* [74].

### 1.4.3.1 Metal nanoparticles in suspension substrates

Suspensions of metal nanoparticles can be prepared by either chemical or physical methods. One physical method is pulsed laser ablation of noble metals in liquid medium [75, 76]. The magnitude of the SERS effect is dependent upon particle

size and the excitation wavelength [77] and the size of the particles depend on the method of preparation.

Wet chemical synthesis of SERS-active nanoparticles is commonly done by reducing silver or gold ions in a solution, usually aqueous media, using reducing agents such as citrate, sodium borohydride, hydrazine, or hydroxylamine hydrochloride [78].

### *1.4.3.1.1 Silver colloid*

Mainly two methods have been used to prepared silver colloidal SERS substrates with suitable physical properties. Silver colloid was prepared by Creighton et al. [79] by reducing aquous solution of silver nitrate ($AgNO_3$) with sodium boro hydride ($NaBH_4$). 15 $cm^3$ of 2 x$10^{-3}$M $NaBH_4$ solution was cooled down to 0°C and stirred rigorously for half an hour. Then 5 $cm^3$ of 1 x $10^{-3}$M $AgNO_3$ solution $AgNO_3$ solution was added drop wise to $NaBH_4$ solution. The mixture was stirred rigorously for 1 hour until glassy yellow color was obtained. The prepared Ag colloidal solution showed a single absorption maximum 396nm (Figure 1.7). The Silver colloid was stored at 5°C and it was stable for several hours.

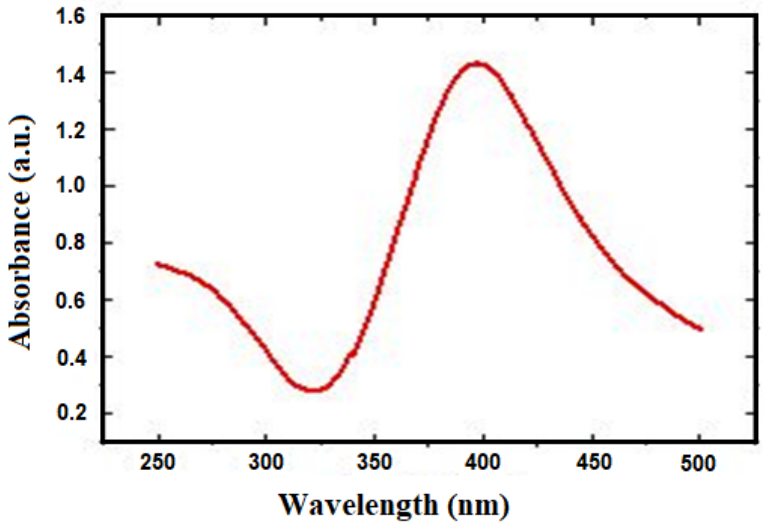


**Figure 1.7**: Extinction spectrum of Ag-sol with absorption maximum at 396 nm [80]

Silver colloid has also been prepared by citrate reduction procedure reported by Lee and Meisel [81]. 500 ml $AgNO_3$ solution was prepared and then this solution was heated to 100C. A 1% sodium citrate was added to 10 ml of $AgNO_3$ solution and the mixture was stirred rigorously. Then it was boiled for 1 hour. The silver colloid showed a single extinction maximum at 425 nm approximately.

### *1.4.3.1.2 Gold colloid*

Gold colloid has been prepared by the following reduction procedure:

1mL 2.5x$10^{-3}$M chloroauric acid ($AuCl_4$) was added to 3 ml 1x$10^{-3}$ M $NaBH_4$ solution. The color of the solution was purple. The gold colloid showed a single extinction maximum at 520 nm approximately [82].

Figure 1.8 depicts UV–vis absorption spectra and absorption shift of gold nanoparticles with different particle sizes [83].

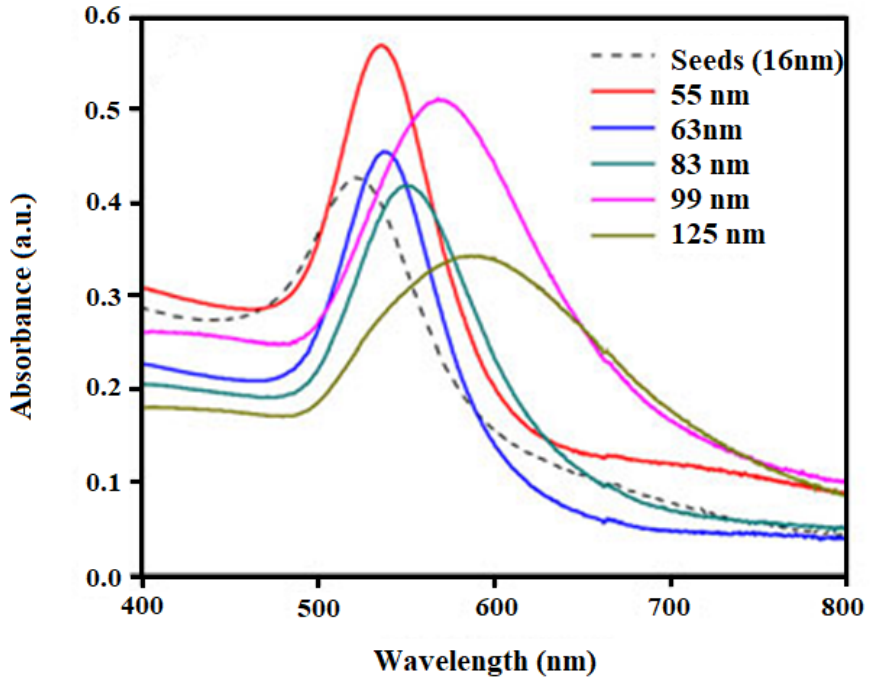


**Figure 1.8**: UV–vis absorption spectra of the synthetized gold nanoparticles [83]

### *1.4.3.1.3 Copper colloid*

Copper colloidal nanoparticles have been prepared [84] by adding 0.1 M copper (II) sulfate pentahydrate solution into 120 mL of starch (1.2 %) solution. The solution was stirred rigorously for 30 minutes. This solution was then added to 50 mL of 0.2 M ascorbic acid solutions and the final solution was then stirred continuously. Subsequently, 30 ml of 1 M sodium hydroxide solution was added to the prepared solution. The mixture was then stirred rigorously and was heated to 80$^{o}$C for 2 hours. The color of the resulting colloid is yellow and it has changed into ocher after 1 hour.

Figure 1.9 depicts that the copper colloid showed a single extinction maximum at 570 nm [85].

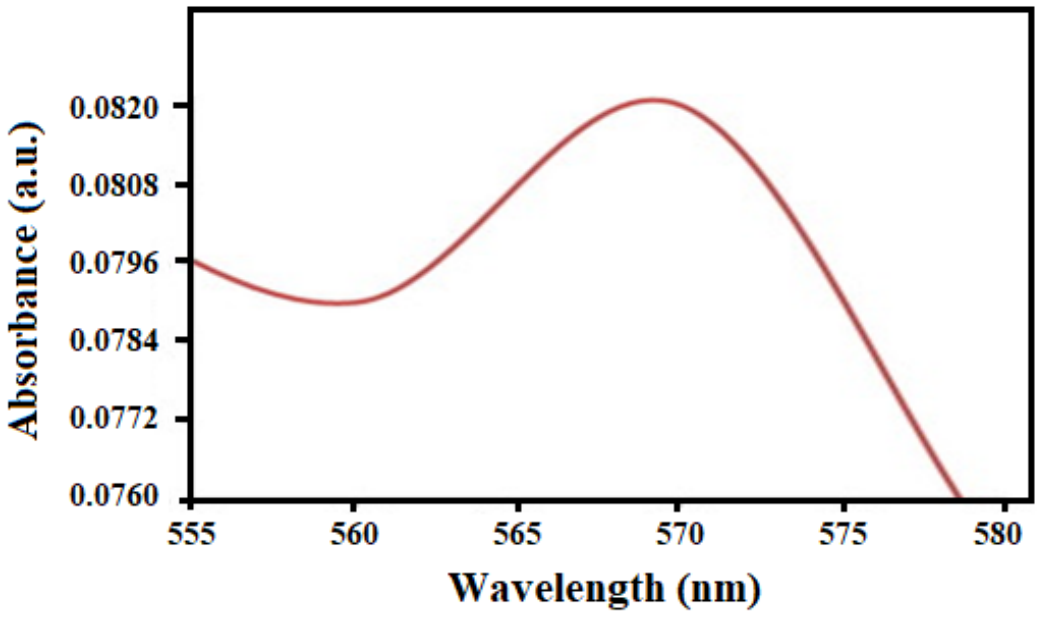


**Figure 1.9**: UV–Visible absorption spectrum of synthesized copper nanoparticles [139]

Currently, there is a growing interest to synthesize copper nanoparticles due to their electrical, catalytic, sensing and surface properties [86-88]. Metallic copper

nanoparticles have been striking materials primarily as they have unique properties [86, 89]. Preparation cost is very low in comparison with the gold or silver nanoparticles [90].
In general, stronger reducing agents, such as sodium borohydride, produce smaller nanoparticles while weaker reducing agents, such as sodium citrate, generate larger particles.

Nanoparticle shape can be controlled by adding surfactants during synthesis [77]. These surfactants will cause a change in surface energy and control particle aggregation. The surfactant stabilizes specific crystal planes in the growing nanostructure thereby allowing controlled growth on that plane.

Depending upon the surfactant and particle material chosen, a wide variety of nanoparticle shapes has been created such as nanorods [77], nanocubes [77, 91], nanospheres [77, 92–94], nanotriangles [77, 91–93], nanowires [77, 91], nanoplates [77, 91], and nanostars [77, 92, 95, 96]. The scanning electron microscopic (SEM) images of some of these surfaces are shown in Figure 1.10 [92].

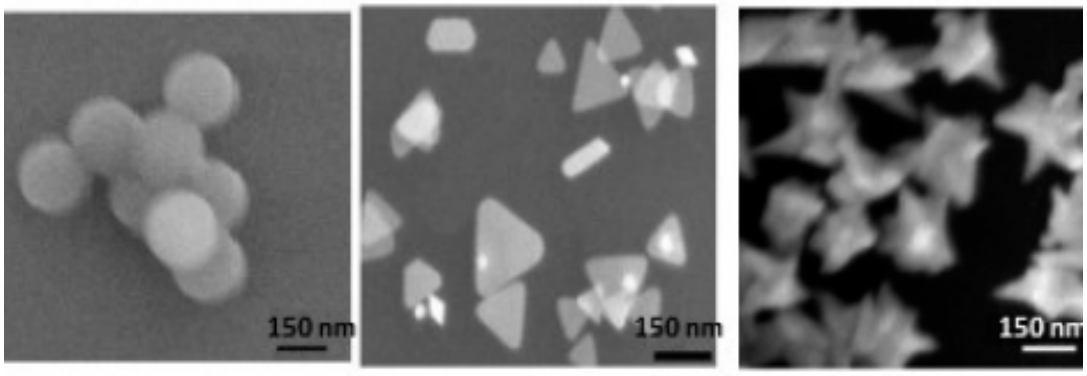


**Figure 1.10:** SEM images of gold nanostructures: (**a**) nanospheres; (**b**) nanotriangles, and (**c**) nanostars [91].

The particle size is significant that determines the SERS enhancement factor. In addition, the shape of the nanoparticles also affects the magnitude of the SERS enhancements [77, 92–94]. SERS spectra of rhodamine 6G adsorbed on gold *nanostars*, *nanotriangles,* and *aggregated nanospheres* are shown in Figure 1.11[92]. The order of the SERS enhancement factors in these nanoparticles is: nanospheres < aggregated nanospheres < nanotriangles << nanostars. In the vicinity of the plasmonic nanostructures there are locations where the local field enhancement is maximum and extremely large compared to that in its surrounding. These locations are named "hot spots" [97]. The dependence SERS enhancement on the shape of the nanostructures is due to the varying number of available "hots pots". The number of intrinsic 'hotspots' per particle increases in the order: nanospheres < nanotriangles < nanostars.

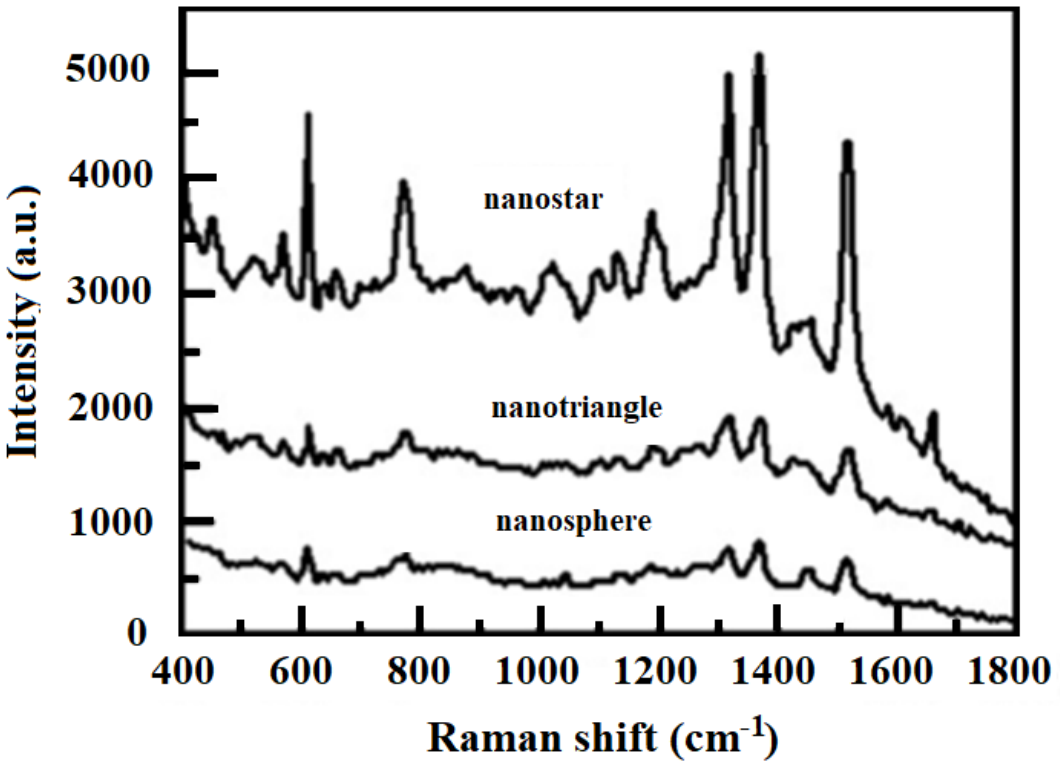


**Figure 1.11.** Comparison of SERS spectra of 5 μM rhodamine 6G in suspensions of gold nanostars, nanotriangles, and aggregated nanospheres. [92].

As the aromatic compounds exhibit strong Raman scattering cross sections, colloidal silver nanoparticles, prepared using wet chemical methods, are suitable for use to obtain SERS spectra of these compounds [98-100].

SERS has also been used to detect compounds like pesticides [101] which do not have aromatic rings but they do contain double bonds that exhibit reasonable Raman scattering cross sections. Detection limits in these cases is found to be in the concentration range $10^{-7}$ – $10^{-4}$ M.

### *1.4.3.1.4 Aggregation of colloidal nanoparticles*

Aggregation of colloidal nanoparticles gives rise to "hot spots" where the local field enhancement is enormous. Controlled aggregation, thus, leads to large SERS enhancement factor. The aggregation is generally initiated by adding suitable reagents to the colloidal suspension of the metal nanoparticles. Also it may take place when the analyte is adsorbed on to the surface of the nanoparticles. Two significant methods of controlled aggregation are cited below:

#### 1.4.3.1.4.1 Microfluidics

Microfluidics has been explored as a means of mixing Ag NPs and samples [102,103]. A schematic of such a device is shown in Figure 1.12a [102]. The detection scheme exploits concentration gradients of chemicals, fostered by the laminar flow in the device, to control the interactions between the analyte, silver nanoparticles (Ag NPs) and a salt.

The Ag colloid used was citrate-capped BioPure 20 nm silver obtained from nanoComposix, Inc. As shown in Figure 1.12a, the device is connected to three reservoirs containing the sample, suspension of Ag NPs, and a salt solution. Flow

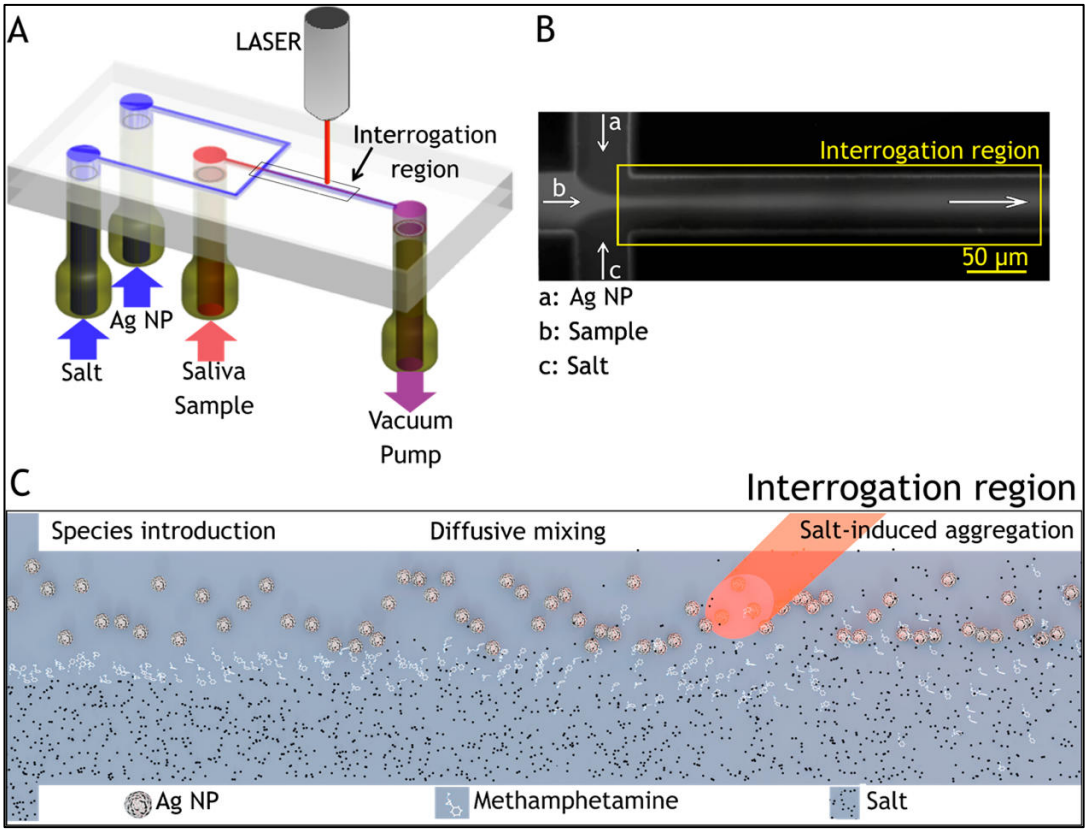


**Figure 1.12.** (**a**) Schematic of the flow-focusing microfluidic device used for controlled Ag-NP aggregation; (**b**) Microphotograph of the flow-focusing junction; (**c**) Schematic of the reactions occurring between the analyte, Ag NPs, and salt ions [102].

through the device is vacuum driven. The spatial arrangement and the flow rate of the three streams have been tailored for optimal SERS detection. Figure 1.12b shows a microphotograph of the flow-focusing junction [102].

Fluorescent dye was used to visualize the sample and side streams to show that diffusion drives lateral mass transport between the laminar flows. A schematic of the reactions occurring in the channel is shown in Figure 1.12c [102]. Ag NPs, analyte, and salt solution are introduced into the channel from the left and flow toward the right. The analyte molecules, introduced through the central stream, diffuse laterally into the side stream containing the Ag NPs thereby allowing the analyte to adsorb on the surface of the Ag NPs. The salt ions induce controlled nanoparticle aggregation, creating SERS-active clusters that convect downstream.

The strongest SERS signal is observed at a location downstream where abundant aggregates reside. It was possible to positively detect/identify the analyte at concentrations as low as 10 nM.

#### 1.4.3.1.4.2 SLIPSERS

Slippery liquid-infused porous surface-enhanced Raman scattering (SLIPSERS) is another means of aggregating nanoparticles in order to increase the magnitude of the SERS enhancement [104].

Figure 1.13a summarizes how SLIPSERS is used. A slippery liquid-infused porous surface (SLIPS) consists of a film of lubricating fluid locked in place by a micro/nanoporous substrate that creates a smooth and stable interface that nearly eliminates pinning of the liquid contact line. Teflon membranes with pore size of 200 nm have been used as the nanoporous substrate and perfluorinated liquids as the lubricating fluid. Perfluorinated liquids are immiscible to both aqueous and nonaqueous phases. A droplet of a suspension of spherical Au NPs and analyte is pipetted onto the surface of the SLIPS. The analyte adsorbs onto the surface of the Au NPs. The droplet evaporates in a constant contact angle mode without noticeable pinning at the contact line, until the particles cluster together to form a 3D aggregate. SERS spectra can then be obtained. Figure 1.13b shows SERS spectra obtained for bis(2-ethyl-hexyl) phthalate (DEHP). DEHP is a contaminant of environmental concern. It is an organic plasticizer commonly absorbed into food and water due to its low vapor pressure. DEHP is only soluble in nonaqueous solvents. Using ethanol as the dispersion medium, it was shown that the SLIPSERS technique was capable of detecting DEHP at sub-femtomolar concentrations. Besides liquid-phase extraction/detection, this platform can also be used for gas-phase and solid-phase extraction/detection.

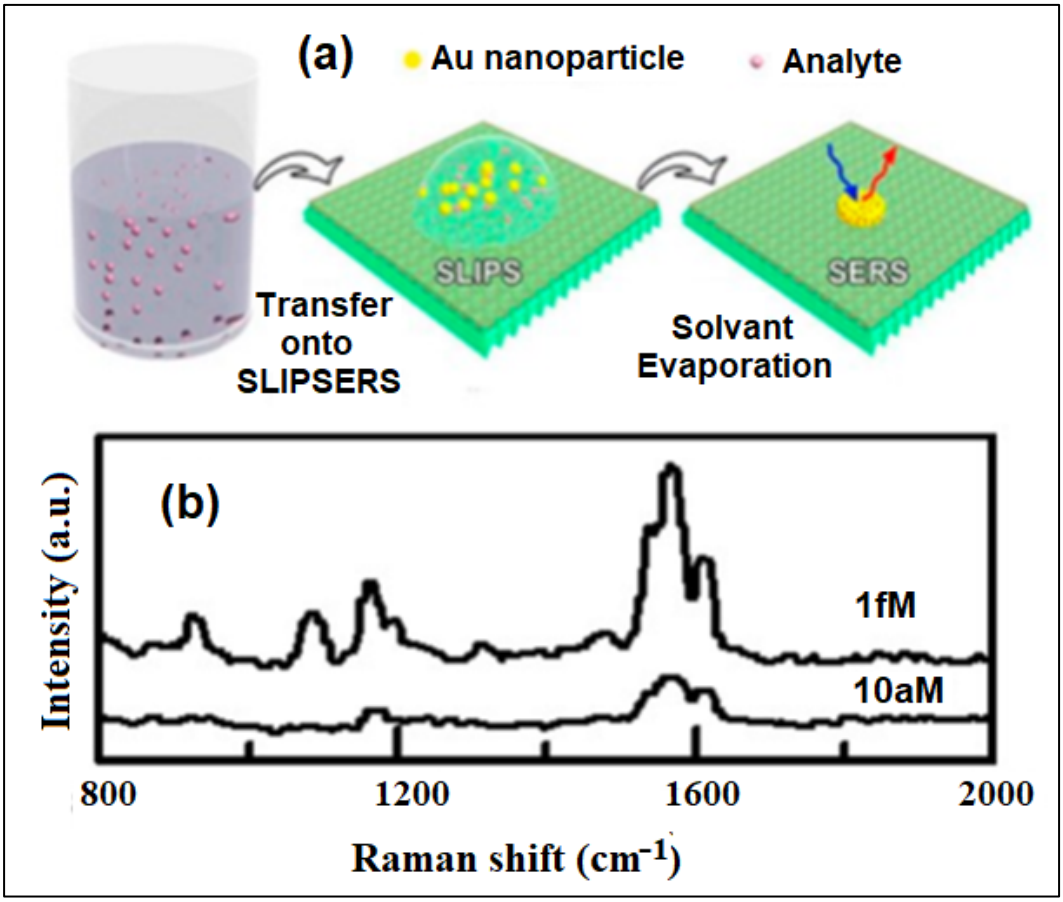


**Figure 1.13.** (**a**) Schematic illustration of the use of SLIPSERS. Au NPs are mixed with analyte to create a suspension. An aliquot of the suspension is placed onto the surface of the SLIPS. As the solvent evaporates, the particles cluster together to form a 3D aggregate consisting of closely packed Au NPs and adsorbed analyte molecules. (**b**) SERS spectra obtained for DEHP in ethanol. An initial volume of 50 µL of analyte solution was used. Concentrations of DEHP are indicated. Spectra were obtained using 633 nm laser excitation [104]

Another way to use suspensions of SERS-active nanoparticles to detect analyte is to mix known amounts of samples with colloidal suspensions and then placing the mixture onto a solid optical substrate. Once dried, SERS spectra are obtained [105].

Although it is very tough to maintain the spacing of the nanoparticles to optimize the SERS activity, the nanoparticles and nanoparticle film electrodes show good surface uniformity. By controlling the inter-particle spacing, template methods can

provide highly uniform SERS substrates. The most widely applicable techniques have been used for the fabrication of SERS are colloids, colloid in sol-gel [106], solid, vapor-deposited metal island films [107], electrochemically roughened electrodes, solution of combustion and lithography produced nanostructures [108] etc.

The serious drawback of all metal colloidal solutions is their instability because they suffer from hardly controlled aggregation (spontaneous or after addition of an adsorbate) which leads to SERS spectral irreproducibility [109].

The surface enhanced property has been influenced by the distribution of sizes and shapes and the ease of aggregation. The silver nanoparticles with appropriate roughness have shown suitable physical properties for an optical electromagnetic field enhancement among all the possible SERS active substrates due to the fractal morphology that result upon their aggregation [110].

### 1.4.3.2 Metal nanoparticles immobilized on solid substrates

#### *1.4.3.2.1 Metal electrodes*

Noble metals like platinum, silver, gold etc. have been used as metal electrodes because of their anodic potential range and favorable electron transfer kinetics [111]. Due to the low hydrogen overvoltage, the cathodic potential range of these electrodes has been restricted. In addition, the kinetics of the electrode reaction has been strongly affected by the high background current due to the formation of surface oxide or adsorbed hydrogen layers. These can be solved by performing a pulse potential cycle before electrochemical experiments [112]. Here, we will briefly discuss several typical metal materials.

Gold and platinum electrodes have good stable chemical properties. Both the materials have easily been obtained and the electrodes can be expediently

manufactured. Silver, which is used for the preparations of chemically modified electrodes in various electrochemical researches, has also been a good electrode surface [113-117]. Silver substrate is directly used for protein analysis as electron will be transformed by these proteins, such as cytochrome c (cyt c) on silver electrode [118].

Some other metals have also been used as electrode substrates besides the noble metal electrodes. For example, the detection of carbohydrates or amino acids in alkaline media can be possible by the construction of copper electrode and nickel electrode. At constant potential, a stable response has been processed by these two kinds of electrodes for carbohydrates in comparison with the gold or platinum electrodes [119].

Also, alloy electrodes have been investigated as SERS substrates. These are often used for the preparation of fuel cells, owing to their bifunctional catalytic mechanism [120].

### *1.4.3.2.2 Metal nanoparticles island films*

The simplest metallic nanostructure can be produced by evaporating a thin layer (less than 10 nm thickness) of a metal such as silver directly onto a solid base support [74]. In this way nanoparticles are formed by the silver layer on the solid in the form of isolated metal islands. A continuous film will be formed by increasing the deposited silver thickness as the particles would start to combine then. The size and shape of the nanoparticles depend on the thickness of the film on the solid support. The thin film showed extension maximum in the range 450-650nm.

Figure 1.14 is an example of the continuous and island thin gold films grown on a glass substrate [121,122]

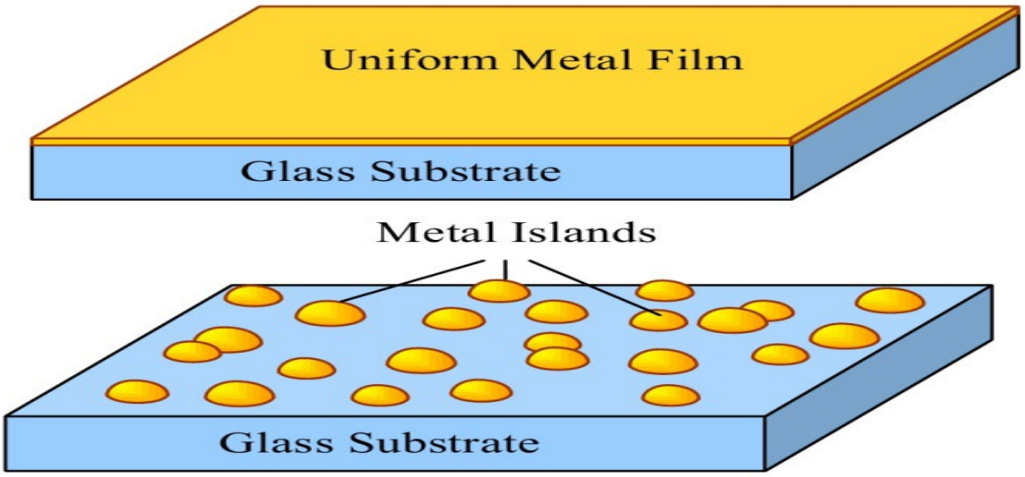


**Figure 1.14:** Continuous metal film and island metal film grown on glass substrates [111, 112]

SERS spectra have been obtained from silver nanoparticles island films and compared with those obtained with other nanostructure materials [123, 124]. SERS spectra of copper and zinc phthalocyanine complexes from silver and indium island films have been reported [125, 126]. After vacuum evaporating of the silver and Indium films onto tetroxide glass slides, the films are coated with copper and zinc phthalocyanine complexes in a vacuum system at a base pressure of $5x10^{-7}$ torr.

In order to produce metal nanoparticles Island films, the thickness of the metal will have to be 7.5 nm on the substrates. By using atomic force microscopy (AFM) the surface roughness and nanometer scale structure of Ag films were characterized by van Duyne et al [127].

### *1.4.3.2.3 Sol-gel process*

The sol-gel method is a wet-chemical procedure and it has been used in material science and ceramic engineering [111]. An integrated three-dimensional network

of materials like metal oxides from a colloidal solution can be fabricated by this technique via hydrolysis and poly condensation reactions [128]. Inorganic silica sol-gel materials have some excellent properties such as high thermal stability, chemical inertness, tunable porosity etc.

Complicated three-dimensional networks of sol-gel can be fabricated by using nano materials. A variety of studies have been conducted from the analysis of protein and cell based on sol-gel technology as because the formed structure of sol-gel matrix can maintain the native functional characteristics of the immobilized proteins [129-134].

### *1.4.3.2.4 Self-assembly monolayers (SAMs)*

Self-assembly is a term to describe processes that a number of spatially disordered objects arrange themselves in an ordered pattern via local interactions. The local interactions are various possible bonds, such as covalent bond, metallic Bond, ionic bond, hydrogen bond, π–π interaction, van der Waals force etc. The self-assembly system has been supported by electrode which can further play more functional roles [74]. Figure 1.15 demonstrates the development a self-assembly monolayer (SAM) on a substrate surface [135].

It is reported that, SAM has been rapidly developed from the late 1980s as the self-assembly is being a widely studied surface modification technology and it is used in molecular biology, material science, medicine [136, 137]. Molecular orientation and packing at the interface between the mono layer and the electrode describe some properties such as injection across the interface [138, 139]. The functions of

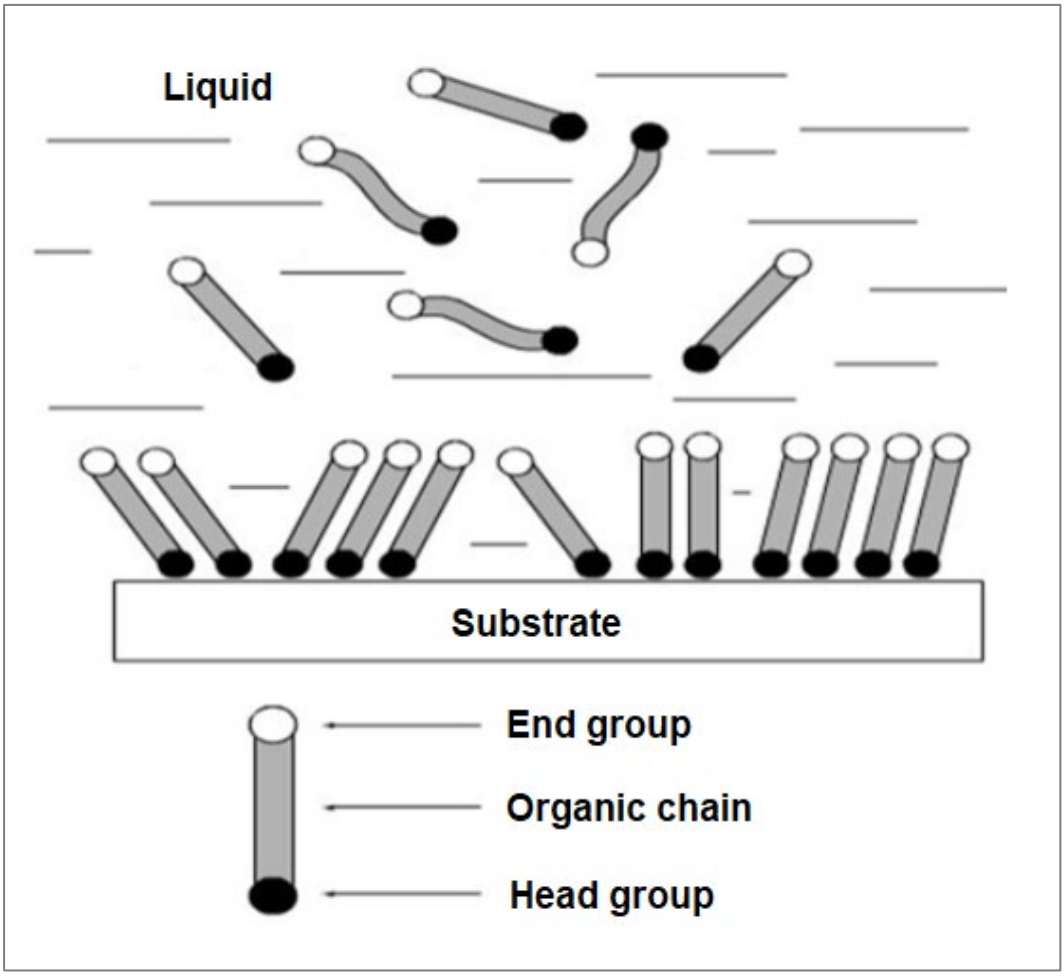


**Figure 1.15**: Schematic representation of the formation of a self-assembly monolayer at a substrate. Reprinted from Ref. [135]

the devices fabricated with SAMs are observed to depend on deposition of the SAMs [140-142].

The advantages of SAM are that the monolayer is chemically stable and biocompatible for electrochemical analysis. The problem of denaturalization of proteins can be overcome by immobilizing the proteins on the SAM-modified electrode. Here the orientation is much more appropriate in comparison with the adsorption on a bare electrode or in a polymer. To assist the formation of a SAM, some inactive reagents have also been used. It is also reported that the rate of the

transfer of electrons between the proteins and the electrode can be largely accelerated by inducing proteins on the mono layers in a suitable orientational manner [143].

### 1.4.3.3 Metal nanostructures fabricated by nanolithography

#### *1.4.3.3.1 Laser ablation*

Recently nanolithography and related nanoimprint lithographic techniques are also employed for the fabrication of highly ordered large-area SERS-active metallic nanostructures. For this purpose, picosecond (ps) and femtosecond (fs) laser pulses are used to ablate solid surfaces [144-148] followed by thin film coating of silver or gold. The metal nanostructures thus obtained, exhibit signal homogeneity, large SERS enhancements factors and chemical stability.


**Figure 1.16**: Schematic representation of the nanosphere lithography process for fabricating metal film over nanosphere (FON), periodic nanoparticle arrays, or nanovoid arrays [155].

An inexpensive technique produce well-ordered 2D periodic arrays of nanoparticles for SERS study is nanosphere lithography (NSL) [149–154].

In this method, generally three types of metal nanostructures [155] are fabricated: (1) Silver or gold film over nanosphere (FON); (2) Array of nanoparticles with a triangular footprint; and (3) Array of uniform sphere voids.

Figure 1.16 summarizes the process. A suspension of monodispersed polystyrene or SiO2 nanospheres, of the desired diameter, is first drop coated onto a clean conductive substrate such as indium tin oxide (ITO) or evaporated metal substrate over glass. The suspension is then dried up. Silver or gold layer of desired thickness is then deposited on the nanospheres. FON and nano array are formed by physical vapour deposition of metal film while the nano voids are obtained by electrodeposition of metal films as illustrated in Figure 1.16.

#### *1.4.3.3.2 Electron beam nanolithography and focused-ion beam nanolithography*

In electron beam lithography technique an accelerated electron beam is focused on an electron-sensitive film called resist to make an exposure. The solubility of the resist is changed due to exposure to electron beam. As a result either the exposed or the non-exposed regions of the resist are removed when the exposed substrate is immersed in a solvent called developer. The template, thus obtained, becomes SERS active as custom patterns of dimension of the orders of 10 nm are formed in this process and the localized surface plasmons (LPS) responsible for the SERS activity are achieved to the desired extent by monitoring the size, shape and arrangement of nanostructure [156-159].

In focused-ion beam nanolithography technique, a beam of accelerated ions, typically gallium ion, strikes the substrate. Because of heavy mass of the ions compared to the electrons, the focused-ion beam directly punch the metal film on

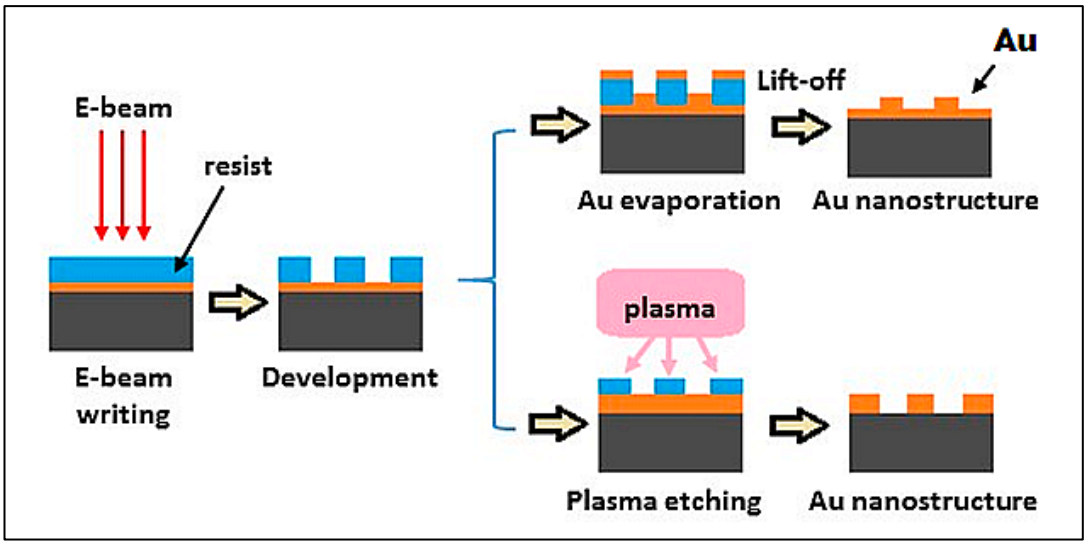


**Figure 1.17:** Schematic diagram of the two fabrication processes used to prepare nanostructured SERS substrates [160, 161].

the substrate thereby resulting in nanostructure of dimension of the order of 5-20 nm [160, 161].

### *1.4.3.3.3 Commercially available SERS substrates*

SERS-active substrates are now commercially available. Of course, most of the manufacturers of these substrates do not expose the details on how these substrates are fabricated. However, many of these commercial substrates are useful as a small volume of sample is required for SERS study with these substrates.

One of the companies marketing SERS-active substrates was *Real-Time Analyzers* [162]. In their 2 mL glass vials, the insides were coated with a SERS-active sol-gel. A solution of the chemical of which SERS study is intended is first injected into the vial and then placed in a Raman spectrometer. Ag or Au sol-gel substrates in capillary tubes and on 96 well microplates are also products of *Real-Time Analyzers*.

Silica coated gold nanoparticles of diameter 5, 10, and 20 nm are being manufactured by *Sigma-Aldrich* [163]. They also produce 10 nm diameter silica coated gold nanobars [164]. These gold nanoparticles and nanobars are fabricated using tetraethyl ortho-silicate (TEOS) and highly branched and mesoporous polymer on the surface of the gold is formed which contains hydroxyl groups that can be used as chemical handles for further functionalization.

Lithography techniques have been used to fabricate commercially available SERS substrates. Dynamic oblique vacuum evaporation technique has been used by *Horiba Scientific* for fabrication of 4mm × 3mm or 5mm × 7mm SERS substrates that are coated with gold nanorods [165].

*Ocean Optics* [166] produces SERS substrates of either a 4mm × 4mm square of Ag/Au film or a 5 mm circle of Ag/Au NPs mounted on a glass slide.

Sputter-coated Ag or Au on a 'plasmonic' substrate created by using ultra-short laser pulses to make nanopatterns on soda-lime glass are the disposable SERS substrates made by *AtoID* [167]. These substrates have to be stored under vacuum and are usable during two months after the manufacturing date.

SERS substrates of *Silmeco* comprises of silicon nanopillars coated with either gold or silver [168–170]. Maskless dry etching is first done to create the silicon nanopillars and then gold or silver is coated on the silicon by electron beam evaporation technique.

*Klarite* substrates developed lithographically by *Mesophotonics* [171] are probably the most characterized SERS substrates. It consists of an array of pyramidal shaped pits etched into silicon [68] followed by coating of a layer of gold. SEM micrograph of a Klarite substrate [172] is shown in Figure 1.18. Roughness of the surface is appropriate for large SERS enhancement factor and the uniformity of the surface enables reproducibility of measurements.

Inexpensive SERS substrates, called P-SERS are the products of *Diagnostic anSERS* comprising of gold nanoclusters, deposited by inkjet printing method, on

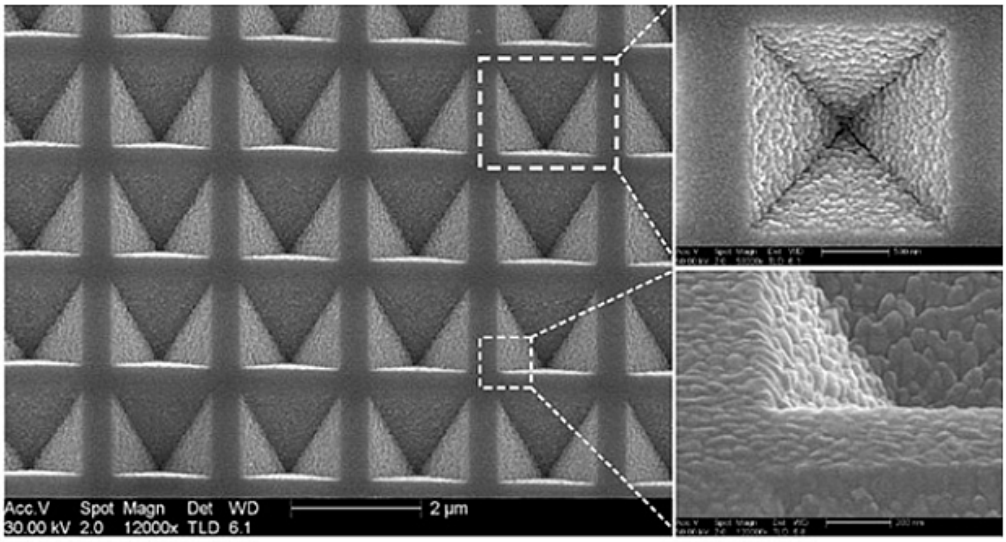


**Figure 1.18:** Electron micrographs ofpyramidal wells in Klarite [172].

the surface of cellulose paper [173-177]. Figure 1.19 shows various available configuration of these substrates [177]. These are flexible substrates. Samples can

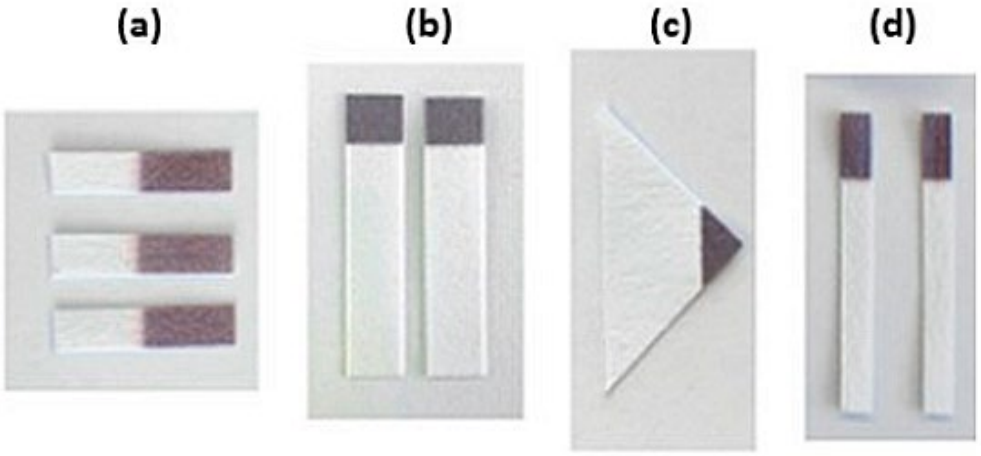


**Figure 1.19:** (**a**–**d**) Different geometries of P-SERS substrates: (**a**) general SERS substrate; **b**) for use in lateral flow concentration experiments; (**c**) for use as a dipstick, and (**d**) for use as surface swabs [177].

be added onto the substrate or the substrate itself can be dipped in the sample or swabbed over the sample. These P-SERS substrates have been used for the detection of drugs, narcotics, pesticides, insecticide residue, and explosives.

## 1.4.4 Mechanisms involved in SERS

The enhancement factor in the SERS signal obtained from molecules adsorbed on the coinage metals silver, gold and copper ranges from $10^6$ to $10^{14}$ depending on the morphology of the surface, chemical nature of the adsorbed molecules and some other factors. This gigantic enhancement needs a theoretical explanation and attempts have been sincerely endeavoured for the purpose since discovery of SERS. Mainly two mechanisms are reported to contribute to the enhancement: a *long-range classical electromagnetic enhancement* and a *short-range first-layer contribution* that is chemically specific and vibrationally selective. The electromagnetic effect is based on the concept that both the incident and the scattered field near the surface are enhanced through surface plasmon resonance whereas the other model involves charge-transfer interaction between the adsorbed molecule and the metal surface, which is most favourable for the molecules directly adsorbed to the surface [178,179].

In case of electromagnetic enhancement mechanism [178], the molecule brought near the SERS-active surface of a metal undergoes coupling with the localized surface plasmon. On the other hand, charge transfer takes place between the adsorbed molecule and the metal surface according to the chemical enhancement mechanism [179].

Assuming two enhancement mechanisms are independent of each other, Xu *et. al.* estimated that the total output photon flux in a SERS experiment can be expressed as [180]

$$\Lambda_{SERS} = \frac{2\pi I_0}{hw_0}\sigma\Sigma_{i=1}^{N} Z_i^{EM} Z_i^{CM} \quad (1.11)$$

Here, $I_0$ is the intensity of the laser beam and $hw_0$ is the laser energy $Z_i^{EM}$ and $Z_i^{CM}$ are the electromagnetic enhancement portion and chemical enhancement portion of the overall enhancement factor respectively. σ is the Raman scattering cross section of the scatterer. The number of scatterer in the probe volume is N.

However, the electromagnetic field enhancement mechanism is observed to be highly dominating over the chemical enhancement mechanism.

### 1.4.4.1 Electromagnetic enhancement mechanism

Electromagnetic field enhancement mechanism will be observed if the molecule gets adsorbed by the metal surface and for this to happen, the roughness of the surface must have to be very high. If a molecule is placed into an electric field E of frequency $\nu$ then oscillating dipole will be induced and the induced dipole moment can be expressed as

$\mu = \alpha E$

The corresponding power ($P_0$) which is generated by the oscillating dipole is proportional to $|\mu|^2$, at the frequency of Raman scattered photon.

In case of SERS, the electric field is modified by the presence of metal nanostructures. Here, local field is enhanced enormously by the plasmon oscillation and thus the power generated by the oscillating dipole is no more proportional to$|\mu|^2$; rather it is modified depending on the nature of the metal and morphology of the surface [152,181].

The local electric field can be expressed as the sum of the incident electric field and an extra field which has been induced during the localized surface plasmon resonance (LSPR) [152] on the surface of the metal. Let $E_L$ be the intensity of this

local field which is much larger than the incident field E in magnitude and opposite in direction to E.

Accordingly, the induced Raman dipole, $\mu = \alpha E$ is enhanced by a factor $M_L(\nu_L) = |E_L(\nu_L)|/|E|$. As a result, the power radiated by Raman dipoles, $P_{Rad}$ will be enhanced by $|E_L(\nu_L)|^2/|E|^2$. The radiation enhancement can be represented as

$$M_{Rad} = P_{Rad} / P_0 \tag{1.12}$$

The total electromagnetic enhancement effect is, of course, a consequence of the enhancement of both the incident electric field and the Raman scattered electric field. Assuming that the enhancement is independent of the absolute photon fluxes and polarizations, *A. Otto* estimated [182] the electromagnetic enhancement factor for a Raman scattering process and the approximated expression is

$$G^{EM}(\boldsymbol{r},\omega) = M_L(\nu_L)M_{Rad} = \left[\frac{E_L(\vec{r},\ \omega)}{E_0(\vec{r},\ \omega)}\right]^2 \left[\frac{E_L(\vec{r},\ \omega_0-\omega_1)}{E_0(\vec{r},\ \omega_0-\omega_1)}\right]^2 \tag{1.13}$$

where,

$E_0$ and $E_L$ are the incident electric field and the total local field respectively;

$\omega_0$ and $\omega_1$ are the frequencies of the incident and scattered radiations respectively

The equation (1.13) can be approximated as

$$G^{EM}(\boldsymbol{r},\omega) =. \left[\frac{E_L(\vec{r},\ \omega)}{E_0(\vec{r},\ \omega)}\right]^4 \tag{1.14}$$

For a particular intensity of excitation, the enhancement factor is governed by $E_L$, the local field which is maximum at the frequency of excitation which results in localized surface plasmon resonance in an isolated metal nanoparticle or in a void or in the aggregate of metal nanostructures. This resonance frequency may depend on the optical properties such as dielectric constant of the material, the size and

shape of the nanostructure or roughness and other variables like small gaps asin bimetallic structures, nanoshells or nanowires. Also, this local field enhancement is maximum for a molecule directly attached to the metal surface (known as the **"first-layer effect"**) and its effect gradually falls off as the distance of the molecule increases from the surface [182].

### *1.4.4.1.1 Surface plasmon resonance*

At the metal-dielectric interface, such as a metal sheet in air, coherent delocalized electron oscillations exist which is known as surface plasmons (SPs). When these SPs are confined in a nanoparticle or in the irregularities of a surface of dimension comparable to or smaller than the excitation wavelength localized surface plasmons (LSPs) are resulted in. The optical absorption of these LSPs is maximum at resonant frequency which is in the visible region for noble metals.

It has now been established that plasmons which are the collective oscillations of the free electrons with respect to the positive ion cores in metals, act as the optical antennas [183] that capture and concentrate light waves. Plasmon oscillations are damped harmonic oscillations, the driving force being that due the external electromagnetic field while the coulomb potential originated from induced charges provides the restoring force [184]. In this case, the damping may be the result of both the emission of radiation and the scattering of carriers by disorder and phonons [185-197]. The resonance frequencies for such damped oscillations are determined by the size [188-190] and shape [190-192] of nanostructure, roughness of the metal surface, dielectric environment [195, 198], chemical composition [194, 199] etc.

However, the plasmon energy of a noble metal can be expressed [181, 197] as

$$\hbar\,\omega_p = \hbar\,[\frac{(n\,e^2)}{(m\varepsilon_0)}]^{\frac{1}{2}} \tag{1.15}$$

where, $\omega_p$ is the plasma frequency. m, e and n represent the effective mass, charge and density of the free electron. $\varepsilon_0$ is the free space permittivity.

The dielectric function of metal is given by simplified Lorentz harmonic oscillator rmodel

$$\varepsilon(\omega) = 1 - \frac{\omega_p^2}{\omega^2 + i\gamma\omega} \tag{1.16}$$

where, γ is a damping constant as a result of electron-electron and electron phonon scattering in the metal. Theses dielectric functions are complex functions and their real and imaginary parts are

$$\varepsilon_1(\omega) = 1 - \frac{\omega_p^2}{\omega^2 + \gamma^2} \tag{1.17}$$

and

$$\varepsilon_2(\omega) = 1 - \frac{\omega_p^2\gamma}{\omega(\omega^2 + \gamma^2)} \tag{1.18}$$

Those metals find plasmonic application for which $\varepsilon_1(\omega)$ has negative values whereas for $\varepsilon_2(\omega)$ has small positive values in the wavelength. In SERS

experiments, the excitation wavelength is generally in the visible and infra-red region and the metals showing large SERS enhancement have value of Reε(ω) as $-20 \leq \varepsilon_1(\omega) \leq -1$.

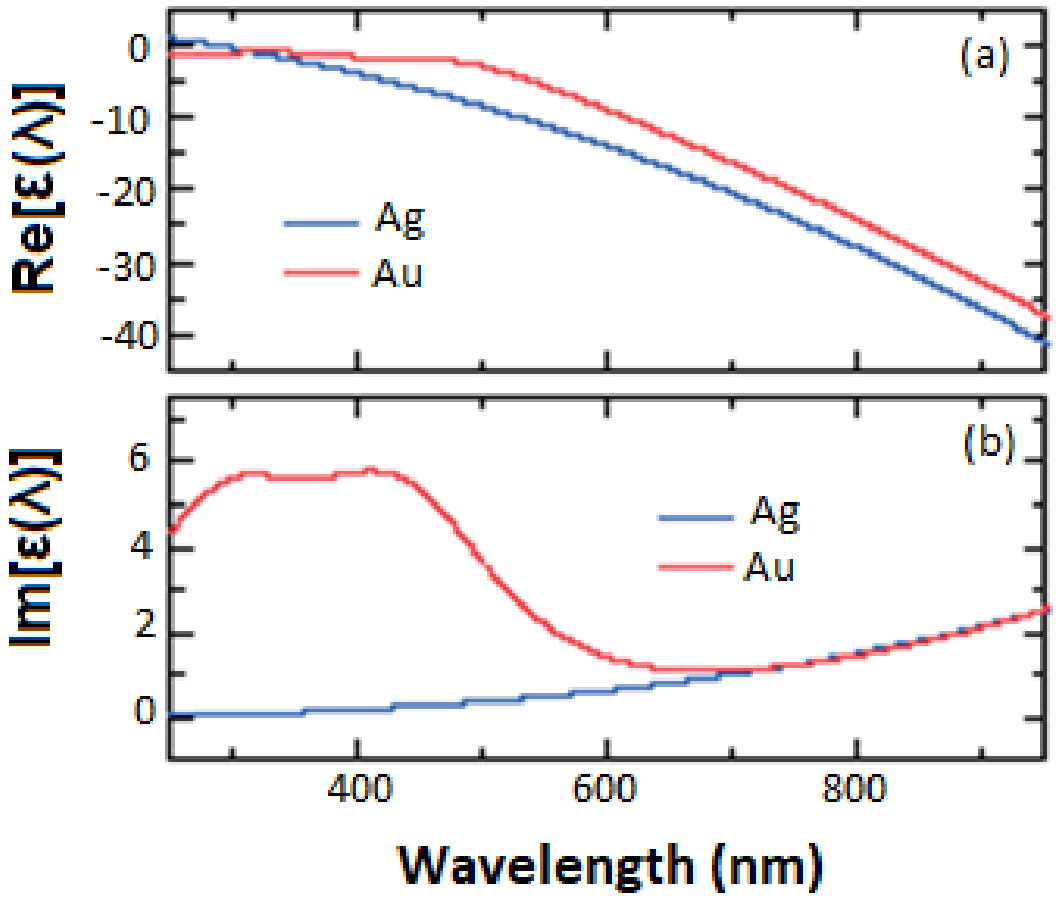


**Figure 1.20:** The real (a) and imaginary (b) parts of $\epsilon(\lambda)$ for Ag and Au.

(Ref: P.G. Etchegoin and Eric C. Le Ru in*: Surface Enhanced Raman Spectroscopy: Analytical, Biophysical and Life ScienceApplications.* S. Schl¨ucker (Eds), WILEY-VCH Verlag GmbH & Co. KGaA, Weinheim, 2011)

Bulk plasmon frequencies belong to the ultraviolet region of an electromagnetic spectrum. However, additional plasmon resonances, known as surface plasmons, are also observed.

Surface plasmon can be classified [181] into surface plasmon polaritons (SPP) and Localized surface plasmon resonances (LSPR).

### *1.4.4.1.2 Surface plasmon polaritons (SPP)*

The oscillations of the conduction electrons at a natural frequency about fixed positive ions in coinage metals such as copper, gold, silver etc. are called plasmons and the natural frequency is called plasma frequency$\omega_p$.

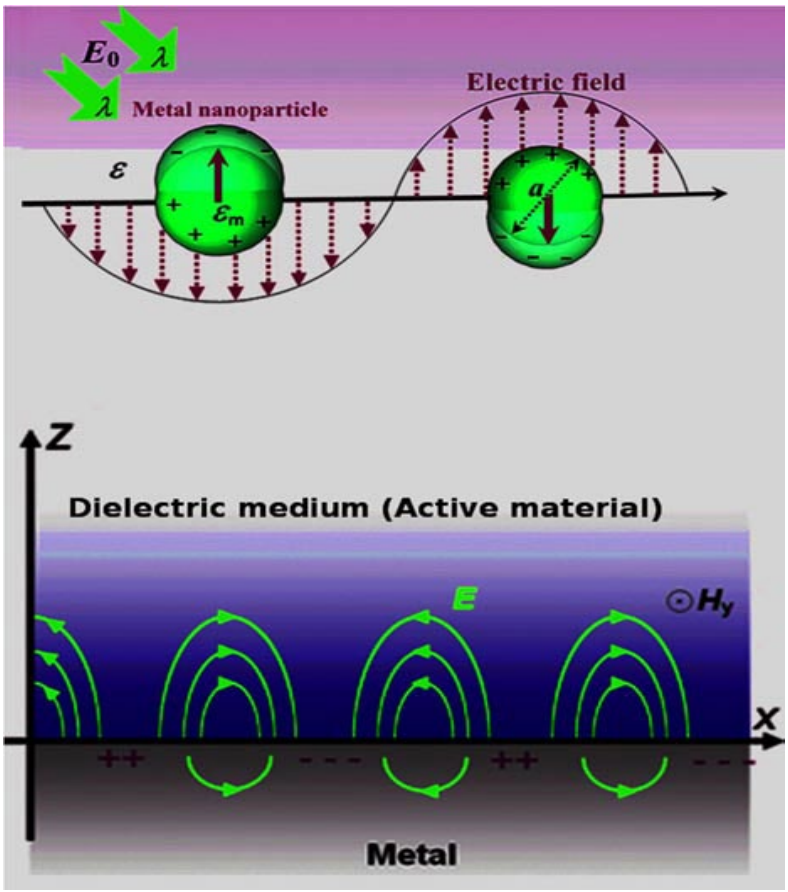


**Figure 1.21:** Schematic diagram of (a) confinement of localized surface plasmons (b) propagating surface plasmon polariton

If a metal is illuminated with light of visible and infrared range, then the photons and the free electron plasmons interact with each other. These mixed modes of photon and plasmon are called surface plasmon polaritons (SPP) [200]. The SPPs are classified into propagating SPP and localized SPP [201-204]. The localized SPP and the propagating SPP are schematically shown in Figure 1.21.

The momentum dispersion relations of surface plasmon polaritons have been well defined. The propagation length is not very high as the surface plasmon polaritons decay in the direction normal to the surface [205]. The electron hole pairs that makeup the SPPs lose energy to phonon scattering which is dissipated as heat. Thus, the SPPs decay by generating heat in the metal [192].

### *1.4.4.1.3 Localized surface plasmon resonance (LSPR)*

The surface plasmons are localized in the metal nano structures when the dimension of the metal nanostructure is comparable to or less than the wavelength of incident radiation. This is designated as localized surface plasmons (LSP) [206]. An explanation of the generation of LSP and the localized surface plasmon resonance (LSPR) may be as follows [200]

In metal nanoparticles, the conduction electrons are partially moving to the lattice of the ionic cores. When electromagnetic field is incident on a metallic structure, the conduction electrons move towards the surface of the metal. Consequently, positive charges are accumulated on the other side of the metal nanoparticle. Electric dipole is thus created which in turn generates an electric field. The direction of the induced field is opposite to that of the incident radiation field. The induced electric dipoles will now oscillate with the natural frequency of the conduction electrons. This natural frequency has been named plasma frequency. If the frequency of the incident radiation field is equal to the plasma frequency then

the induced dipole will oscillate with maximum amplitude. This situation is called localized surface plasmon resonance (LSPR).

The LSPR can produce electric field ten times stronger than the incident field. As the accumulation of the charges on the metal surface vary with different shape and morphology, the resonance conditions also vary with different dielectric environment, nanoparticle size etc.

The schematic diagram of LSPR and spatial distribution of the induced electric field around the nanoparticle is shown [207] in Figure 1.22.

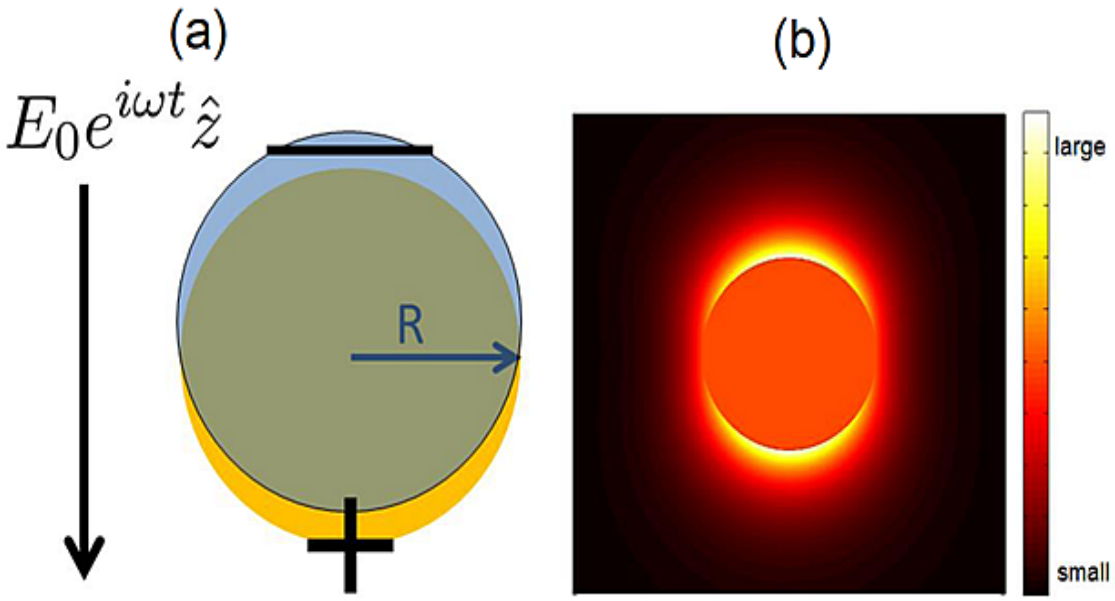


**Figure 1.22: a)** Illustration of a localized surface plasmon resonance (LSPR). An oscillating electric field displaces the electron cloud (blue) with respect to the positive background ions of a metallic nanoparticle. b) Spatial distribution of the induced electric field around the nanoparticle. [199]

### *1.4.4.1.4 Estimated enhancement factor for metallic nanostructures*

Coherent oscillation of the conduction electrons sets in when a small spherical metallic nanoparticle is irradiated by light. This collective oscillation of the electrons is called the dipole plasmon oscillation. The oscillation frequency depends on the density of electrons, the effective mass of the electron and the shape and size of the charge distribution.

The dipole plasmon oscillation frequency may be related to the dielectric constants by considering a single spherical metal nano particle [208] (radius of the nano particle is small compared to the wavelength of light). As the radius a is very much small, compared to the wavelength of incident light λ, the electric field is uniform over the nanoparticle. Under this condition, Maxwell's equation may be replaced by Laplace's Equation [209] of electrostatics to determine the outside and inside field of the sphere. Considering the incident light to be z-polarised, the resulting field outside the sphere ($\overline{E}_{out}$), can be expressed as [208],

$$\overline{E}_{out} = E_0 \hat{z} - \alpha E_0 \left[\frac{\hat{z}}{r^3} - 3\frac{z}{r^5}(x\hat{x} + y\hat{y} + z\hat{z})\right] \quad (1.19)$$

Here, the first term represents the incident field and the second term is the induced field due to the dipole. α is the metallic polarizability and can be represented as

$$\alpha = g\, a^3 \quad (1.20)$$

where, a is the radius of the particle and g is given by

$$g = \frac{\varepsilon_{in} - \varepsilon_{out}}{\varepsilon_{in} + 2\varepsilon_{out}} \quad (1.21)$$

$\varepsilon_{in}$ and $\varepsilon_{out}$ are the dielectric constant of metal nano-particles and external environnement respectively.

The enhancement will be maximum when the real part of $\varepsilon_{in}$ approaches to-$2\varepsilon_{out}$with very small imaginary part.

According to Mie theory, the intensity distribution, for metal nano particles of arbitrary shape, in the extinction spectrum is given by [210, 211]

$$E(\lambda) = \frac{24\pi^2 N a^3 \varepsilon_{out}^{3/2}}{\lambda \ln 10}\left[\frac{\varepsilon_i(\lambda)}{(\varepsilon_r(\lambda)+\chi\varepsilon_{out})^2+\varepsilon_i(\lambda)^2}\right] \quad (1.22)$$

where, $\varepsilon_r$ and $\varepsilon_i$ are the real and imaginary components of the metal dielectric constant $\varepsilon_{in}$, respectively. $\varepsilon_{out}$ is the dielectric constant of the external environment. $\chi$ is the shape factor of the metal nanostructure and for sphere [212], $\chi = 2$. Therefore, the localized surface plasmon resonance (LSPR) can be generated [212, 213] by putting the condition $\varepsilon_r = -\chi\varepsilon_{out}$.

If the size of the metallic nano-particles increases i.e. if the radius is not comparable or less than the wavelength of the incident light, the electric field is no more uniform over the metallic nano particle. In that case, multipolar terms (($l = 2$) need to be included in addition to the dipole oscillation [208].

The Raman scattering intensity is proportional to $E_0^2$, where $E_0$ is the peak value of intensity of the electric field in the incident light [214]. In SERS, the incident field is enhanced significantly and thus the SERS intensity may be approximated to vary as the absolute square of $\overline{E}_{out}$, evaluated at the surface of the spherical metal nano-particles (i.e. at r=a).

Using equations (1.19) –(1.21), it can be shown that $\overline{E}_{out}$ is given by,

$$\left|\overline{E}_{out}\right|^2 = E_o^2\left[|1-g|^2 + 3\cos^2\theta\left(2\mathrm{Re}(g)\right) + |g^2|\right] \quad (1.23)$$

where, $\theta$ is the angle between the incident electric field vector and position vector $\bar{r}$. Maximum enhancement will take place when $\theta = 0^0$ or $\theta = 180^0$.

When g is very large, the enhancement approaches the value

$$\left|\overline{E}_{out}\right|^2 = E_0{}^2 |g|^2 (1+ 3\cos^2\theta) \quad (1.24)$$

Therefore, at $\theta = 0^0$ or $\theta = 180^0$, the peak in enhancement will have the value [142]

$$\left|\overline{E}_{out}\right|^2 = 4\, E_0{}^2 |g|^2 \quad (1.25)$$

The radially averaged intensity [152] is given by,

$$\left|\overline{E}_{out}{}^{av}\right|^2 = 2\, E_0{}^2 |g|^2 \quad (1.26)$$

Sometimes in Raman scattering, the radiation from the oscillating dipole may have some Stocks shifted values due to the vibrational frequency of the molecule. Therefore, the output radiation field from the dipole will be enhanced. By considering this fact, the equation (1.23) needs modification. The proper treatment of this complicated modification has been done by Kerker *et al*. [215, 216].

However, proceeding with equation (1.23), the theoretical SERS enhancement factor can be estimated, the approximate value of which is given by,

$$EF = \frac{|E_{out}|^2 \left|E'_{out}\right|^2}{|E_0|^4}$$

$$= 4\, |g|^2\, |g'|^2 \quad (1.27)$$

where the prime symbols refer to the field evaluated at the Stokes scattered frequency. Equation (1.27) is identical to the equation that has been derived by Kerker *et al*. [215, 216].

Now, Stokes-shifts being small, the $|g|$ and $|g'|$ will be maximum at the same wavelength. Therefore, $EF \approx |g|^4$. It is also known as $E^4$enhancement at the surface of the nano-particles.

For small sphere, if $|g|$ is approximately ten in magnitudes, then the electromagnetic enhancement will be $10^4$ to $10^5$, and the electromagnetic enhancement will be $10^8$, if the value of $|g|$ is much larger in higher-order silver nanostructures [217].

### 1.4.4.2 Chemical enhancement mechanism

Several evidences suggest that, an individually different enhancement mechanism has also been observed alongside the electromagnetic enhancement mechanism in a particular system. Both the mechanisms are simultaneously operative and multiplicative in nature in a common SERS spectrum. In order to ensure chemical enhancement effect, the molecule must have to be adsorbed directly to the roughened surface of the metal [13]. The direct contact of the molecule to the metal causes a charge transfer between the metal and the molecule. This charge transfer mechanism is a short-range effect and it depends upon the energy levels of both the metal and adsorbate, their bonding nature etc [218, 219].

The coupling between the metal and the molecule increases the Raman scattering cross section of the molecule. The chemical enhancement mechanism can be classified as [200] SERS of chemically bonded molecules with charge transfer resonance, SERS of chemically bonded molecules without charge transfer resonance, SERS of physisorbed molecules and surface enhanced resonance Raman scattering (SERRS).

Chemical enhancement mechanism can be explained by resonance Raman mechanism [13] in which either (i) the interaction between the metal and the molecule leads to the broadening and shifting of the electronic state of the adsorbed molecule or (ii) some new intermediate molecular states arises by chemisorption in Raman scattering.

The absorption of a photon by the metal leads to a dynamic charge transfer which results in a hot electron state [74]. It should be mentioned that the highest occupied molecular orbital (HOMO) and the lowest unoccupied molecular orbital (LUMO) of the adsorbed molecule is symmetrically disposed in energy with respect to the Fermi level of the metal [13]. The charge transfer process can be classified into two parts [74], molecule to metal and metal to molecule charge transfer process. In molecule to metal charge transfer excitation, an electron is transferred from the HOMO to the Fermi level of the metal. In metal to molecule charge transfer excitation, an electron is transferred from Fermi level of the metal to the LUMO. Therefore, the Raman signal will be increased due to the increase of the LUMO electrons as the probability of the electron photon coupling in the Raman scattering tensor increases. The LUMO electrons are then transferred back to the metal and the excess energy is released in the form of Stokes photons. This mechanism is known as first layer effect [220]. The chemical enhancement will be maximum if the molecule is attached directly to the metal surface.

Chemical enhancement is best explained by resonance Raman scattering theory [74]. When the molecule is irradiated by a radiation with energy which is equal to one of the electronic transitional energy in the molecule, resonance Raman scattering takes place. Matrix elements involving wave function overlap of localized electron density of states are favourable near the Femi level and thus Lombardi *et al*. assumed that transitions from states near the Femi level are preferred and described the whole process to take place in four steps [220]. (1) The incident radiation with energy $h\nu_0$ first creates an electron hole pair in the metal and the electron is thus excited as a "hot electron".

(2) This "hot electron" then occupies a vacant level in the adsorbed molecule, preferably the LUMO thereby giving rise to an excited charge transfer state.

(3) After perturbing the electronic states of the adsorbed molecule by creating an adsorbate molecule-electron negative ion, the "hot electron" returns to the metal.

(4) Electron, returning to the metal, recombines with the hole which was created in step (1) and this recombination leads to a vibrationally excited neutral molecule. During this process, Raman shifted photons of energy hν (say) is released.

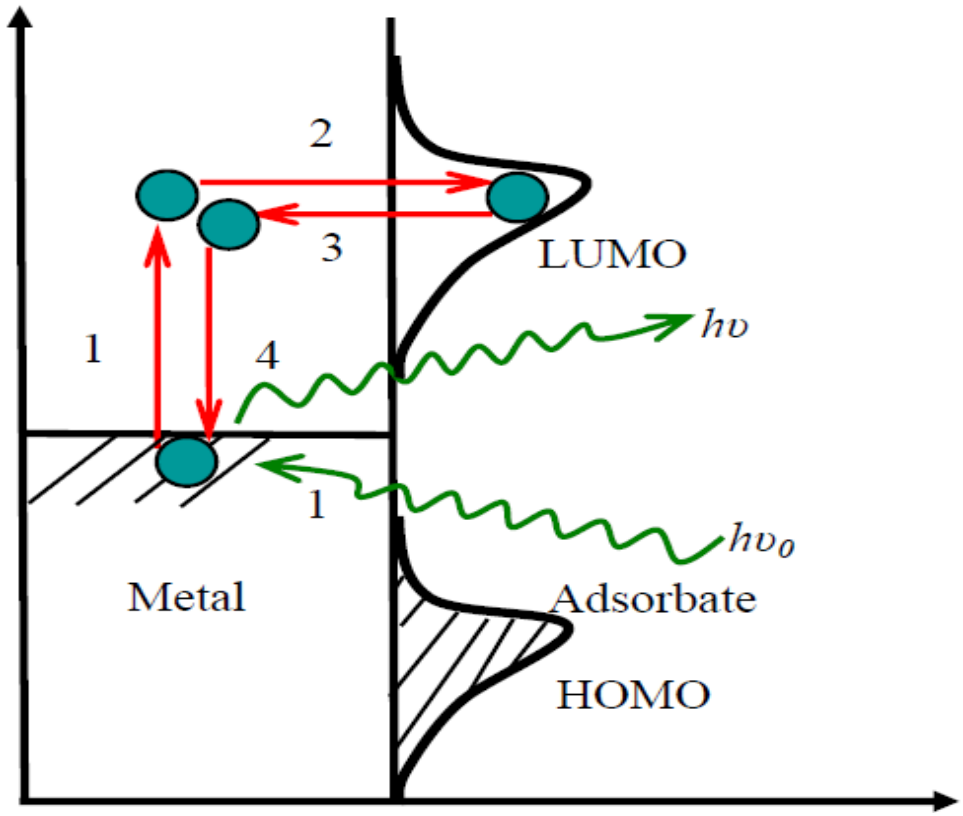


**Figure 1.23**: Schematic diagram of the four-step process of the photon driven charge transfer model for a molecule adsorbed on an electrode [221, 222]

Figure 1.23 depicts the operative charge transfer mechanism for a molecule adsorbed on an electrode [221, 222].

Lombardi *et al* [220] presented an explanation of the chemical enhancement mechanism and estimated a contribution to SERS intensities based on the Herzberg-Teller coupling mechanism. Figure 1.24 shows the scheme of the explanation where $M_{IM}$ and $M_{MK}$ represent matrix elements corresponding to molecule-to-metal and metal-to-molecule charge transfer transitions.

The matrix elements $M_{IM}$ and $M_{MK}$ tend to zero when the distance between molecule and metal is large. However, the molecule and metal combine to form a single system when the molecule is chemisorbed on to the metal surface forming a weak chemical bond. In that case, these matrix elements will have non-zero values. In this combined system the vibronic mixing of metal states with ground and excited states is also taken into account by considering the matrix elements $h_{IM}$ and $h_{KM}$.

In Figure 1.24 I and K are two discrete molecular levels between which a transition is assumed to be allowed. The continuous metal level of the conduction band of the metal ranges between $\omega_A$ and $\omega_B$ and is assumed to have a constant density of states $\rho_0$. The filled levels range up to $\omega_F$, the Fermi level, and are depicted by lines, while the unfilled levels are depicted by dots.

It has been suggested [220] that, in molecule to metal charge transfer excitation, charge transfer takes place between the ground molecular state and unfilled levels of the metal (Figure 1.24. (b)). In this transition, intensity is borrowed from the allowed transition by means of vibronic coupling between metal levels and the excited molecular level which is represented by the matrix element $h_{MK}$. In case of metal to molecule charge transfer excitation, charge transfer takes place between the filled levels of the metal and the excited molecular state (Figure 1.24. (c)). Energy for this transition is obtained from the allowed transition by means of vibronic coupling between metal levels and the ground molecular state through the matrix element $h_{IM}$.

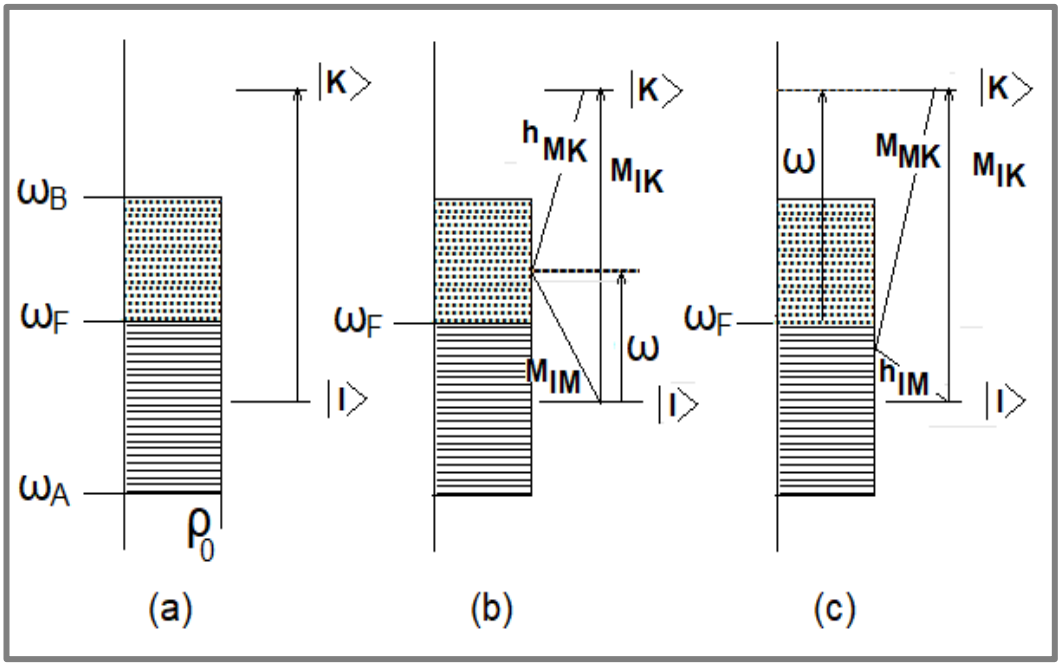


**Figure 1.24:** (a) Energy level scheme for molecule-metal system. (b) Molecule to metalcharge transfer transitions(c) Metal to molecule charge transfer transitions

In the charge transfer process, electronic levels of both the metal and molecule are involved [74]. The position of the Fermi level is dependent on the applied potential. Therefore, by changing the applied potential one can get the maximum enhancement. The direction of charge transfer depends on the change of the Fermi level by the applied potential and corresponding energy level shifting. For red-shifts charge transfer will take place from a filled metal orbital to an empty absorbed orbital and the reverse is the case for blue shift [223, 224].

Although the contribution of chemical enhancement mechanism has only the factor of 10 $-10^2$ compared to the factor of $10^4$–$10^7$ for electromagnetic enhancement mechanism, it is extremely imperative, however, to recognize the chemical mechanism for its significance to analytical applications, because the output SER spectra cover the evidence about the molecule and its environment, for example, its

interactions with the metal surface, its spatial alignment along with the polarization properties of the local electric filed [13, 74].

## 1.4.5 Application of SERS

SERS is now being used for the detection of wide range of analytes at low concentration [225-227], including but not limited, to pollutants [228], explosives [229,230], chemical warfare agents [231], and DNA [232]. Both the colloidal dispersion of metal nanoparticles and the nanostructures immobilized on solid surface are used for SERS detection. In the former case, the analytes are homogeneously absorbed onto the metallic nanoparticles and in the latter the absorption is heterogeneous.

SERS technique is not only capable of the confirmatory identification but the detection may be quantitative [233, 234]. For quantitative SERS detection the analyte may be measured simultaneously with different concentrations of an "internal standard" [235]. A calibration curve is first drawn with the known concentrations of the "standard" and then is used to determine the concentration of the analyte provided that both the internal standard and the analyte have similar or equal adsorption affinity to the metal surface and the vibrational "fingerprints" of the internal standard does not overlap with the Raman spectrum of the analyte. Shen et. al. used 4-mercaptopyridine as the internal standard and 1,4-phenylene diisocyanide, uric acid, and basic red 9 as the analytes for quantitative SERS measurements [236].

Recently, quantitative SERS measurements at the single-molecule level have been reported on an Ag-nanoparticle-based SERS substrate by Chen *et. al.[*237].

SERS has now become a powerful analytical technique in various research areas that include forensics and medicine also. Application of SERS has found its place even in biomedical imaging facilities like magnetic resonance imaging [MRI] and

into clinics [238]. It is now possible to detect as well as identify bacteria in urine and serum using SERS techniques [239, 240].

### 1.4.5.1 Spectro-electrochemistry and catalysis

Low-intensity visible light can be concentrated and channelized on the adsorbed molecule by plasmons of the SERS substrate and thus plasmon-driven photocatalysis (PDP) is possible [241, 242]. Besides PDP, a wide and miscellaneous range of chemical applications of SERS has been reported [243]. SERS has many applications on catalysis [244] and electrochemistry [245-247]. The analyte molecules range from diatomic [247] and aromatic compounds [248, 249] to proteins attached to model membranes [250-253].

Plasmonic activity and catalytic activity are normally two distinct functionalities. If the nanoparticles (NPs) present in colloidal suspensions can integrate these two functionalities

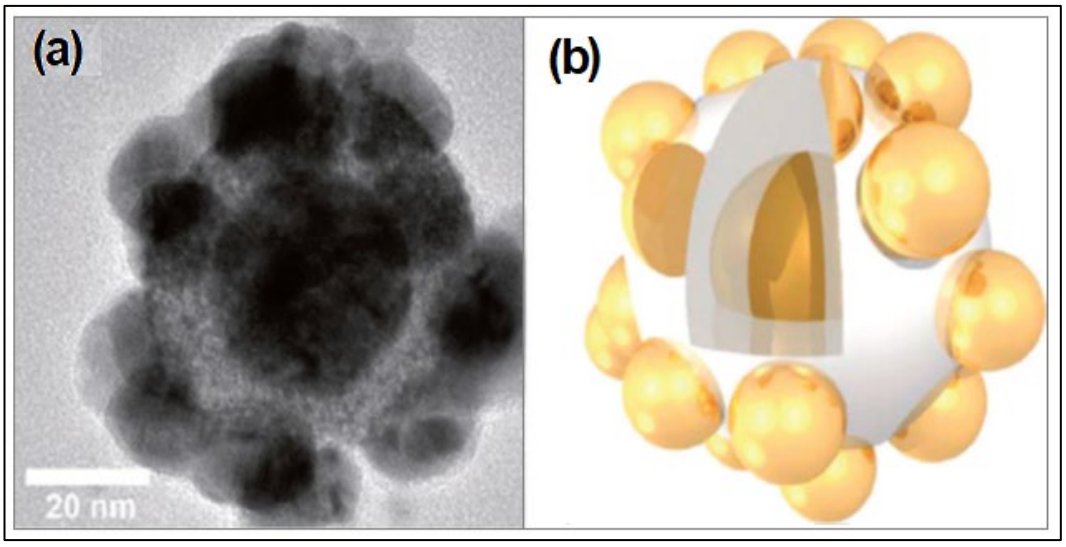


**Figure 1.25**: a) HR-TEM image of a Au/Pt/Au Nano raspberry and b) a computer-generated 3D model [249].

into a single bifunctional entity, SERS can monitor the catalytic reactions [243]. It is thus, challenging to design and synthesize hybrid metal nanostructures that display high SERS action and a huge surface area of the catalytically active metal.

To fulfill these criteria, the raspberry-shaped Au/Pt/Au core/shell NPs have been prepared for platinum-catalyzed reactions [249] as depicted in Figure 1.25. An HR-TEM image (Figure 1.25(a)) of a solo raspberry shaped NPs along with a computer-generated 3D model of the core/shell geometry with large Pt surface area (Figure 1.25(b)) are shown.

Here, the 80 nm Au core shell is SERS-active when isolated whereas the small Pt protuberances are not effectively SERS-active in isolated state. However, plasmonic coupling takes place between these two types of nanoparticles and the entire superstructure achieves plasmonic activity and at the same time the surface area is significantly increased which is required for catalytic activities. The hybrid model, thus, combines the plasmonic activity and catalytic activity rendering itself bifunctional [243].

The raspberry-shaped Au/Pt/Au core/shell NPs have been used to study the hydride reduction of an aromatic nitro compound, 4-nitrothiophenol, to the corresponding aniline derivative as revealed by SERS shown in Figure 1.26. The characteristic nitro (R—$NO_2$) peaks are observed to decrease and on the other hand the azo bands (R—N=N—R) initially increase and then finally disappear with increasing amount of $NaBH_4$ (from bottom to top).

SERS study of the same nitro compound was carried out with a mixture of bare Au and Pt nanospheres. In this case combined catalytic/SERS activity has not been the result. The quantification of the contributions of nitro, azo, and aniline compounds in each SERS spectrum is possible by decomposing the spectrally overlapping contributions from all three species with nonnegative matrix factorization.

Oxygen electroreduction has long been the focus of electrochemical research because of its important role in corrosion and fuel cells. SERS finds application to

study intermediates connected with the electroreduction of molecular oxygen on bismuth-modified polycrystalline Au surfaces which serve as a model system [247].

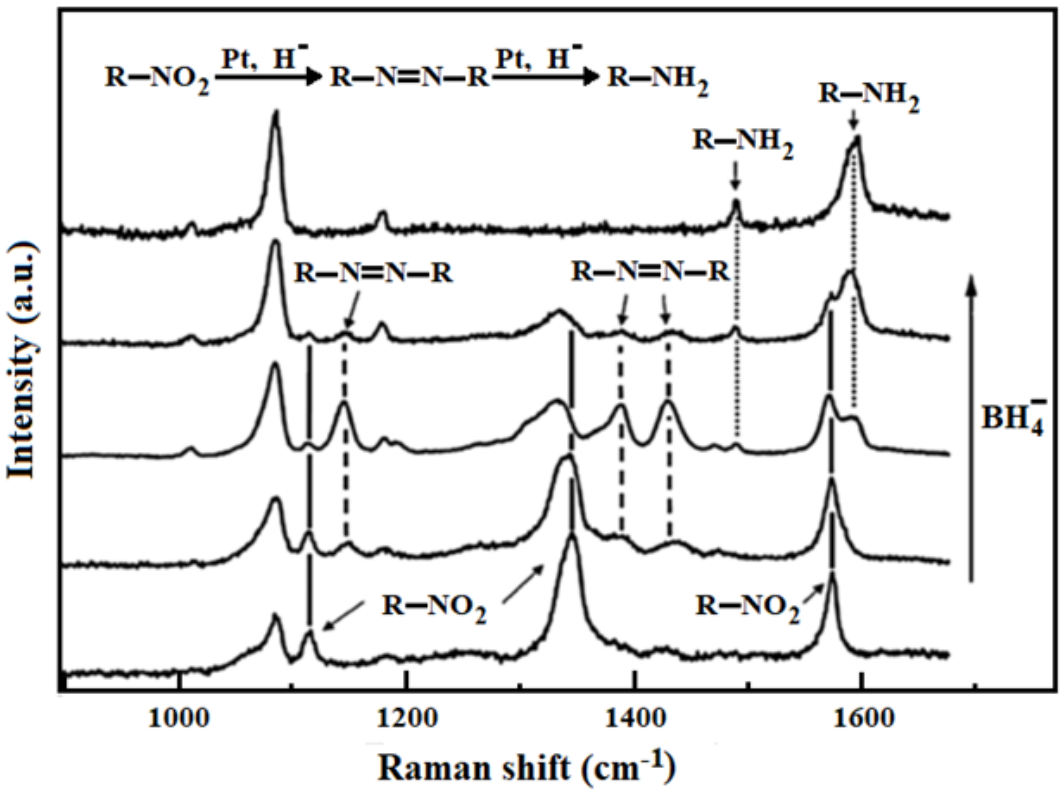


**Figure 1.26**: SERS spectra have been recorded for the Pt-catalyzed hydride reduction of 4-nitrothiophenol to the corresponding aniline derivative using Au/Pt/Au Nano raspberries [249].

### 1.4.5.2 Single-molecule detection

It is of great scientific and practical interest in diverse field of research like chemistry, biology, medicine, pharmacology, and environmental science to detect single molecule in solution with high sensitivity and molecular specificity [254,255]. In the process of human gene analysis selective and rapid detection of single molecules is of great importance [255].

Detection of single molecule means obtaining spectroscopic signal from $1.66\times10^{-24}$ ($1/N_A$) mol of a substance and for this purpose the molecule concerned should have extraordinary absorption or emission properties.

Nie and Emory [256] and Kneipp et al. [257] demonstrated by their seminal observations that it is possible to achieve single-molecule detection using SERS and/or SERRS (Surface enhanced resonance Raman spectroscopy). Single rhodamine 6G molecules adsorbed on selected nanoparticles was achieved by Nie and Emory [254] using SERS techniques. They first screened individual silver colloidal nanoparticles from a large heterogeneous population for the purpose. Single-molecule SERS (SM-SERS) was successfully carried out by Kneipp et al. for the detection of single crystal violet molecule in aqueous colloidal silver solution [257].

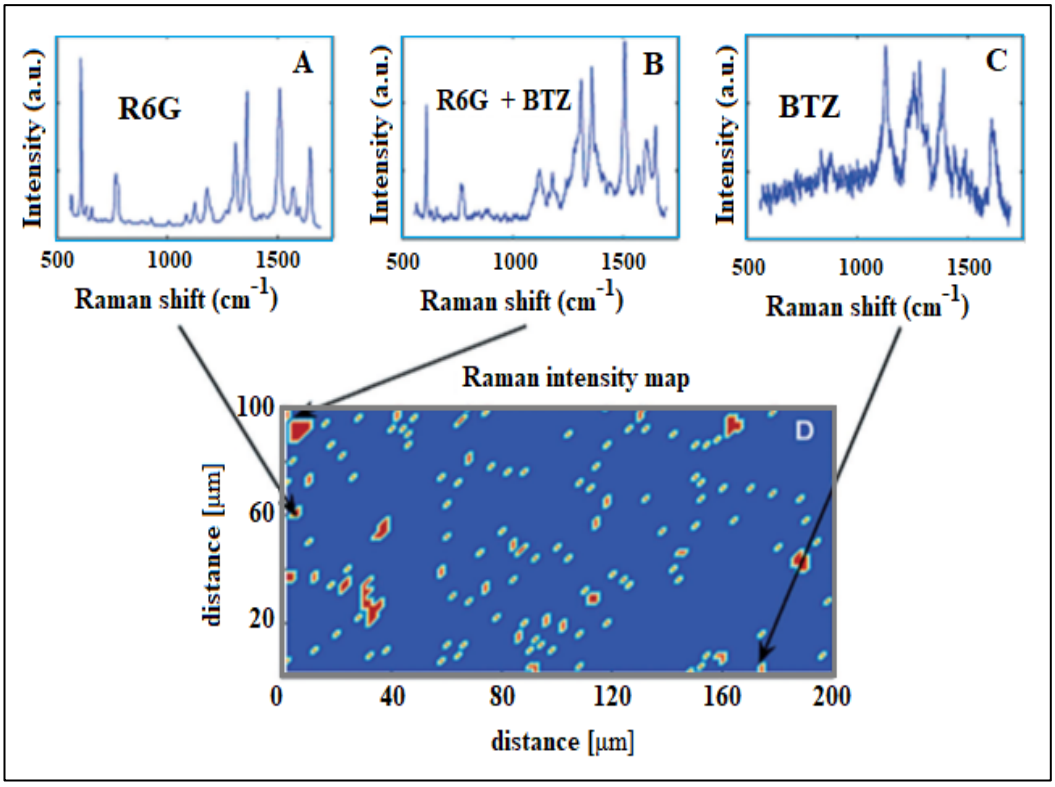


**Figure 1.27**: Bianalyte SERS (BiASERS) for the wavenumber-domain based demonstration of single-molecule SERS. From Ref. [258].

These approaches of single-molecule detection have been convoyed by some difficulties such as, low dye concentrations, strong intensity variations etc. under different circumstances [258-260]. Le Ru et. al. [258] proposed a method of simultaneous use of two analyte molecules having clearly distinguishable SERS spectra to confirm the single (or few)-molecule nature of the signals which eliminates most of the uncertainties associated with low dye concentrations. This bianalyte approach has been termed as BiASERS. A colloidal solution was prepared with a mixture of equal concentrations of rhodamine 6G (R6G) and benzotriazole (BTZ) (100 nM for each dye) and also individual solutions of R6G and BTZ (100 nM for each dye) were prepared for SERS studies. In a separate experiment it has been confirmed that the two dyes do not interact with each other and adsorb on the colloids independently of each other. Figure 1.27 (A) and Figure 1.27 (C) respectively show SERS spectra of R6G and BTZ while Figure 1.27 (B) shows a combination of both, pulled out from different locations of a SERS micro spectroscopic test (bottom).

For a single molecule (either R6G or BTZ), the ratio of the finding probability is 1:1. In case of two molecules, the probability distribution of having either 2R6G or 1R6G/1BTZ, or 2BTZ will be 1:2:1. In the similar process, the finding probability of the individual molecule will decrease by increasing the number of molecules.

### 1.4.5.3 Glucose sensing

Diabetic patients suffer from unusual production or performance of insulin that maintains desired glucose level in blood. The fluctuation of blood glucose contents gives rise to a number of complications in the functioning of kidney, heart, eye, nerves and blood itself. The usual method of measurement of their glucose levels is by indirect electrochemical detection of hydrogen peroxide produced by enzymatic oxidation of glucose in the collected blood samples. With a view that a faster, easier, and less painful method for frequently measuring glucose levels would be of great individual, clinical, and societal benefit, many groups are researching

methods for minimally invasive, biologically compatible, quantitative glucose detection [261,262].

Direct detection of glucose using SERS has been attempted and quantitative glucose sensing has been possible by employing silver film over nanosphere (AgFON) as the SERS substrate [260].

As in high performance liquid chromatography (HPLC) self-assembly monolayer (SAM) is used to create the stationary phase [263-267], R.P. van Duyne et. al.[260] used a partition layer over AgFON (Figure 1.28a) in order to stabilize the Ag surface against oxidation and to preconcentrate the analyte by the synthetic control of the partition layer. Of the twelve SAMs they tried, only the straight chain alkanethiols, especially 1-decanethiol (which forms a monolayer on silver ~1.9 nm thick) [268], were found to be effective partition layers,

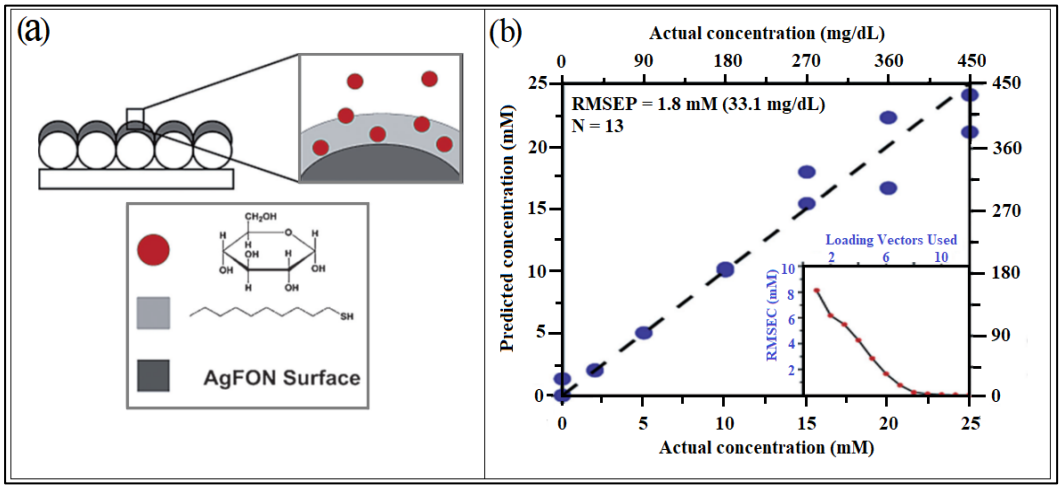


**Figure 1.28**: (a) Sensing glucose on AgFON with 1-decanethiol partition layer. (b) Concentration-dependent SERS measurements of glucose [260].

Leave-one-out (LOO) [269] partial least-squares (PLS) [270,271] analysis has been employed to demonstrate quantitative glucose detection (Figure 1.28b) both over a large (0-250 mM) and clinically relevant (0-25 mM) concentration range. The root-mean-squared error of prediction (RMSEP) of 1.8 mM (33.1 mg/dL) in the clinical study is near that desired for medical applications (1 mM, 18 mg/dL).

### 1.4.5.4 Cancer detection

Cancers are of different types in respect of manifestations, prognosis, steps and severity of sign and symptoms but in general abnormal proliferation and growth of involved organ or organ cells are the main causes of it which spread from the point of origin to other parts of the body. For actual treatment of cancer, initial detection is vital. Positron emission tomography, computer tomography, MRI etc. are some powerful procedures established for cancer detection [272]. Application of Raman spectroscopy in detecting cancer is a new possibility. As normal Raman signal are generally weak, SERS seems to be more skilled for this purpose [273,274] among the several methods based on Raman.

Day *et. al*. [275] have designed a Raman probe with novel design that is small enough to fit down the biopsy channel of an endoscope and enabling rapid evaluation of tissue with a penetration depth of approximately 200µm (Figure 1.29)

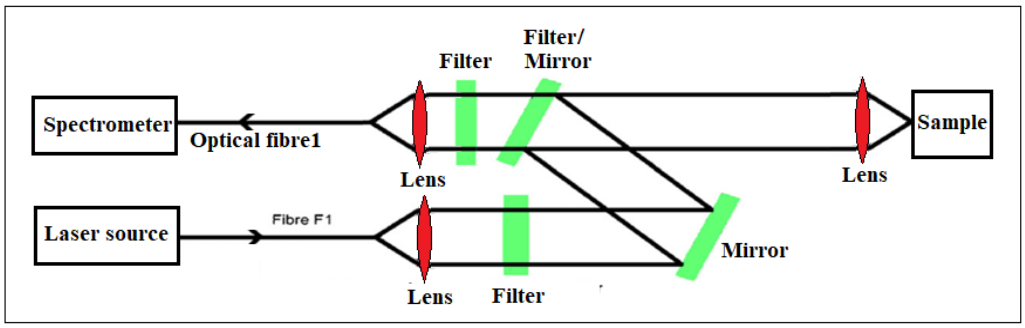


. **Figure 1.29.** Optical layout of the miniature confocal Raman probe.

Breast cancer is the most common cancer in women and after lung cancer, the second most dominant cancer causing deaths after lung cancer in overall [276]. To spot normal, precancerous and cancerous breast tissues, quite a lot of researches have used RS. Maximum studies have been done on breast cancer recognition focusing on EGFR (epidermal growth factor receptor). Magnification of human EGFR2 or human epithelial receptor 2 (HER2) has been a prognostic marker in several types of cancers [274, 277-281]

Gold nano popcorn (GNPOP)-attached single wall carbon nanotube (SWCNT), a novel hybrid nanomaterial was designed and used for targeted diagnosis [282]. It was observed that S6 aptamer attached GNPOP-modified SWCNT based SERS assay is highly selective for binding with SKBR3 as a human breast cancer cell line, which overexpresses human

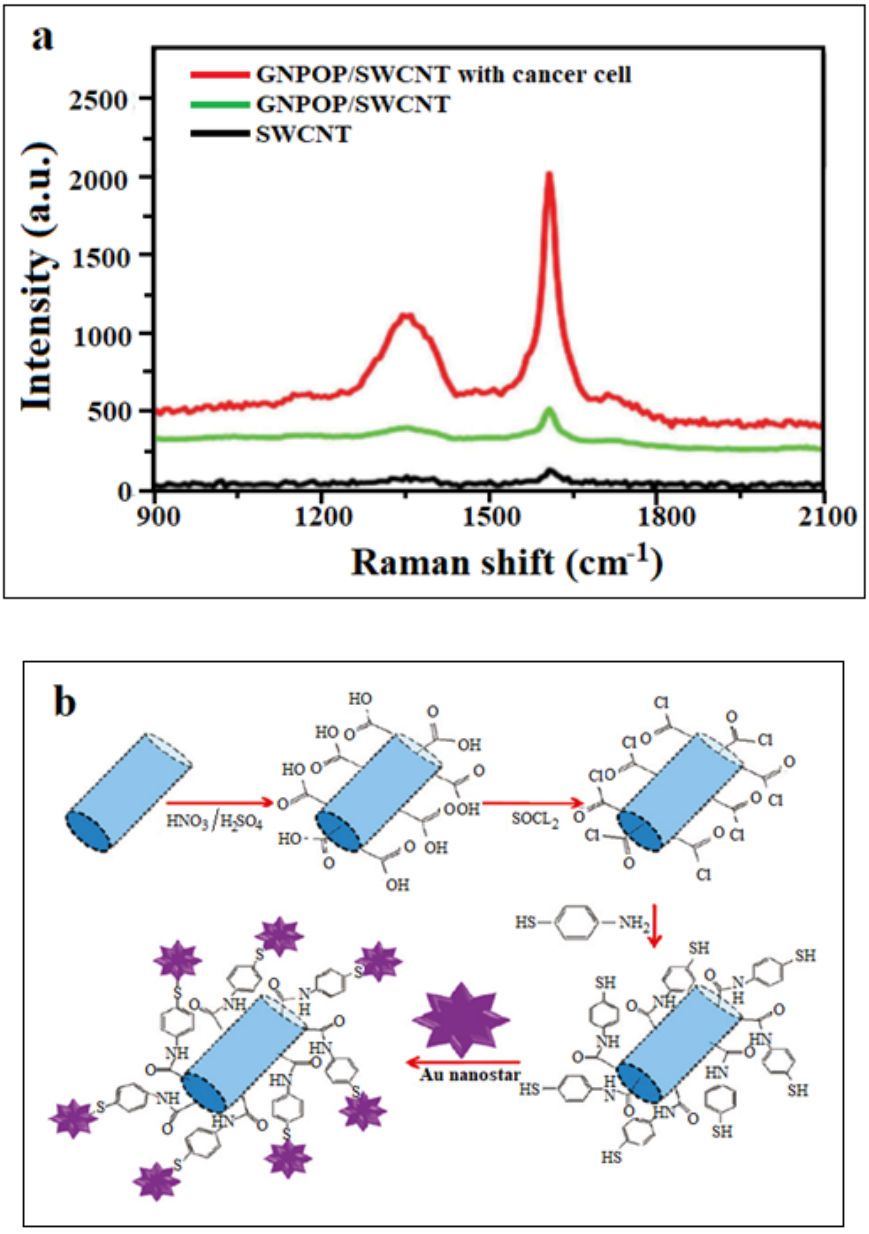


**Figure 1.30** :a) Plot showing SERS. (b) Schematic representation shows the synthesis of GNPOP attached SWCNTs [282]

epithelial receptor 2 (HER2). The selective binding in MDA-MB cell (This cell line was derived at M.D.Anderson in 1976. Here MDA stands for "M.D. Anderson and MB stands for Metastasis Breast cancer") as HER2-negative breast cancer cell linewas also compared [272, 282]. GNPOPs are capable of providing enhancement of Raman signals by several orders of magnitude and it showed the ultrasensitive detection capability and it has enormous potential for applications in cancer cell detection from clinical sample [282].

SERS has also been used for detection of colorectal cancer. In order to decrease the fluorescence background from the bulk tissues, Maghemite ($Fe_2O_3$, $\gamma$-$Fe_2O_3$) nanoparticles have been manufactured by Campos da Paz et al. [283] precoated with dimercaptosuccinic acid. The cell lines expressing characteristic carcinoembryonic antigen (CEA) of colorectal cancer (CRC) cells have been aimed by the surface, which functionalized with anti carcinoembryonic antigen (anti-CEA). Then, the surface decoration of the nanosized maghemite particles have been traced by SERS from the initial precoating up to the attachment of the anti-CEA moiety [283].

SERS could also be used to detect brain cancer. Aydin et al. [284] reported that a 60-nm gold core has been covered with the Raman molecular tag trans-1,2-bis(4-pyridyl)-ethylene and this Raman active surface is protected by a 30 nm silica coating. The particles then were modified with 1,4,7,10-tetraazacyclododecane-1,4,7,10-tetraacetic acid in complex with $Gd^{3+}$ ((DOTA)-$Gd^{3+}$) using a maleimide linkage (maleimide-DOTA-Gd). The high-resolution brain tumor imaging and picturing of the margins of an invasive tumor were then demonstrated by this technique [284,285].

Suitable designing of various nanostructures can ensure sensitivity and specificity of cancer detection [286, 287].

# References


[1] M. Fleischmann, P.J. Hendra and A.J. McQuillan, *Chem. Phys. Lett.*, **26** (1974) 163.

[2] K. Kneipp, Y. Wang, H. Kneipp, L.T. Perelman, I. Itzkan, R.R. Dasari and M.S. Feld, *Phys. Rev. Lett.*, **78** (1997) 1667.

[3] A. Smekal, *Naturwissenschaften*, **11** (1923) 873.

[4] C. V. Raman and K. S. Krishnan, *Nature*, **121** (1928) 501.

[5] R. Dua (http://rishidua.com/RishiDua_2010EE50557.pdf.)

[6] C.N.Banwell, *Fundamentals of Molecular Spectroscopy*., McGRAW-HILL Book Company.

[7] H.W. Schroetter and H.W. Kloeckner in: *Raman Spectroscopy of Gases and Liquids* (Springer, Verlag, Berlin, 1979).

[8] B. Schrader and D.S. Moore, *Pure Appl. Chem*., **69** (1997) 1451.

[9] E. L. Ru and P. Etchego in: *Principles of Surface-Enhanced Raman Spectroscopy and Related Plasmonic Effects* (Elsevier, Oxford, UK, 2009).

[10] K. Eberhardt, C. Stiebing, C. Matthäus, M. Schmitt and J. Popp, *Expert Rev. Mol.Diagn.*, **15** (2015) 773.

[11] D.J. Jeanmaire and R.P. VanDuyne, *J. Electro. Anal. Chem*., **84** (1977) 1.

[12] M. G. Albrecht and J. A. Creighton, *J. Am. Chem. Soc*., **99** (1977) 5215.

[13] A. Campion and P. Kambhapati, *Chem. Soc. Rev*., **27** (1998) 241.

[14] M. Moskovits, *J. Raman Spectrosc*., **36** (2005) 485.

[15] T. Vo-Dinh, *TrAC. Trnds Anal. Chem*., **17** (1998) 557.

[16] D.C. May, X. S. Zheng, K. Weber and J. Popp **,** *Chem. Soc. Rev.***, 46** (2017) 3945.

[17] J.R. Lombardi and R.L. Birke*, J. Phys. Chem*. C, **112** (2008) 5605.

[18] K. Kneipp, Y. Wang, H. Kneipp, L. T. Perelman, I. Itzkan and M. S. Feld, *Phys. Rev. Lett.,* **78** (1997) 1667.

[19] F.J. Adrian, *J. Chem. Phys*., **77** (1982) 5302.

[20] P. Avouris and J.E. Demuth, *J. Chem. Phys*., **75** (1981) 4783.

[21] A.M. Michaels, M. Nirmal and L.E. Brus, *J. Am. Chem. Soc*., **121** (1999) 9932.

[22] M. Moskovits, *Phys. Chem. Chem. Phys*. **15,** (2013) 5301.

[23] K. Carron, L.Peitersen and M. Lewis, *Environ. Sci. Technol*., **26** (1992) 1950.

[24] P. A. Mosier-Boss and S. H. Lieberman, *Anal. Chim. Acta*., **488** (2003) 15.

[25] L. E. Kreno, N. G. Greeneltch, O. K. Farha, J. T. Hupp and R. P. Van Duyne, *Analyst,* **139** (2014) 4073.

[26] C. Qian, Q. Guo, M. Xu, Y. Yuan and J. Yao, *RSC Adv*., **5** (2015) 53306.

[27] O. Péron, E. Rinnert, M. Lehaitre, P. Crassous and C. Compère, *Talanta,* **79** (2009) 199.

[28] O. Péron, E. Rinnert, T. Toury, M. L. de la Chapelle and C. Compère, *Analyst*, **136** (2011) 1018.

[29] L.G. Olson, R.H. Uibel and J. M. Harris, *Appl. Spectrosc*., **58** (2004) 1394.

[30] P.A. Mosier-Boss and S.H. Lieberman, *Anal. Chem*., **77** (2005) 1031.

[31] K. Mullen and K. Carron, *Anal. Chem*., **66** (1994) 478.

[32] P.A. Mosier-Boss and S.H. Lieberman, *Appl. Spectrosc*., **57** (2003) 1129.

[33] W. Wang and B. Gu, *Appl. Spectrosc*., **59** (2005) 1509.

[34] B. Gu, C. Ruan and W. Wang, *Appl. Spectrosc.,* **63** (2009) 98.

[35] C. Ruan, W. Wang and B. Gu, *Anal. Chim. Acta*, **567** (2006) 114.

[36] B. Gu and C. Ruan, *Anal. Chem*., **79** (2007) 2341.

[37] C. Ruan, W. Luo, W. Wang and B. Gu, *Anal. Chim. Acta*, **605 (**2007) 80.

[38] A.M. Jubb, P.B. Hatzinger and B. Gu, *J. Raman Spectrosc*., **48** (2017) 518.

[39] P.A. Mosier-Boss and M.D. Putnam, *Anal. Chim. Acta*, **801** (2013) 70.

[40] P.A. Mosier-Boss and M.D. Putnam, *Spectrochim. Acta*, **133** (2014) 156.

[41] S. Gajaraj, C. Fan, M. Lin and Z. Hu, *Environ. Monit. Assess*., **185** (2013) 5673.

[42] P.A. Mosier-Boss and S.H. Lieberman, *Appl. Spectrosc*., **54** (2000) 1126.

[43] P.A. Mosier-Boss and S.H. Lieberman, *Appl. Spectrosc*., **55** (2001) 1327.

[44] W. Wijaya, S. Pang, T.P. Labuza and L. He, *J. Food Sci.*, **79** (2014) T743.

[45] A. Kim, S.J. Barcelo and Z. Li, *Nanotechnology*, **26** (2015) 015502.

[46] J. Kubackova, G. Fabriciova, P. Miskovsky, D. Jancura and S. Sanchez-Cortes, *Anal. Chem.,* **87** (2015) 663.

[47] Y. Zhang, Z. Wang, L. Wu, Y. Pei, P. Chen and Y. Cui, Analyst, **139,** (2014) 5148.

[48] H. Zhang, Y. Kang, P. Liu, X. Tao, J. Pei, H. Li and Y. Du, *Anal. Lett*., **49** (2016) 2268.

[49] R.A. Sulk, R.C. Corcoran and K.T. Carron, *Appl. Spectrosc*., **53** (1999) 954.

[50] S.C. Cînta Pînzaru, I. Pavel, N. Leopold and W. Kiefer, *J. Raman Spectrosc*., **35** (2004) 338.

[51] O. Alharbi, Y. Xu and R. Goodacre, *Analyst*, **139** (2014) 4820.

[52] S. Mabbott, O. Alharbi, K. Groves and R. Goodacre, *Analyst*, **140** (2015) 4399.

[53] O. Alharbi, Y. Xu and R. Goodacre, *Analyst,* **140** (2015) 5965; *Nanomaterials*,, 7 (2017) 142

[54] K. Dana, C. Shende, H. Huang and S. Farquharson, *J. Anal. Bioanal. Tech*., **6** (2015) 1000289.

[55] N.A. Hatab, G. Eres, P.B. Hatzinger and B. Gu, *J. Raman Spectrosc*., **41** (2010) 1131.

[56] A. Chou, E. Jaatinen, R. Buividas, G. Seniutinas, S. Juodkazis, E.L. Izake and P.M. Fredericks, *Nanoscale*, **4** (2012) 7419.

[57] H. Wackerbarth, C. Salb, L. Gundrum, M. Niederkrüger, K. Christou, V. Beushausen and W. Viöl, *Appl. Opt.*, **49** (2010) 4362.

[58] P.M. Fierro-Mercado and S.P. Hernández-Rivera, *Int. J. Spectrosc*., **212** (2012) 716527.

[59] S. Botti, S. Almaviva, L. Cantarini, A. Palucci, A. Puiu and A. Rufoloni, *J. Raman Spectrosc.*, **44** (2013) 463.

[60] K.T. Carron and B.J. Kennedy, *Anal. Chem*., **67** (1995) 3353.

[61] D.A. Heaps and P.R. Griffiths, *Appl. Spectrosc*., **59** (2005) 1305.

[62] J.M.L. Sequaris and E. Koglin, *Anal. Chem*., **59** (1987) 525.

[63] R.D. Freeman, R.M. Hammaker, C.E. Meloan and W.G. Fateley, *Appl. Spectrosc*., **42** (1988) 456.

[64] B.J. Kennedy, R. Milofsky and K.T. Carron, *Anal. Chem*.**, 69** (1997) 4708.

[65] N. Wei_enbacher, J. Frank and H.D. Wanzenböck, *Analyst***, 123** (1998) 1057.

[66] P.A. Mosier-Boss and S.H. Lieberman, *J. Electroanal. Chem*., **460** (1999) 105.

[67] M.R. Bailey, A.M. Pentecost, A. Selimovic, R.S. Martin and Z.D. Schultz*, Anal. Chem*., **87** (2015) 4347.

[68] G. McNay, D. Eustace, W.E. Smith, K. Faulds and D. Graham, *Appl. Spectrosc*., **65** (2011) 825.

[69] T.V. Dinh, *Trend. Anal. Chem.*, **17** (1998) 558.

[70] Z.Q. Tian, *J. Vib. Spectrosc*., **4** (2000) 2.

[71] D.S. Wang and M. Kerker, *Phys. Rev*., **24** (1981) 1777.

[72] Z.Q. Tian, Z.L. Yang, B. Ren, Wu and D.Y. Top., *Appl. Phys*., **103** (2006) 125.

[73] Z.Q. Tian, Z.L. Yang, B. Ren, D.Y. Wu in: *Surface-enhanced Raman scattering: physics and applications, Top. Appl. Phys.* **103***,* (K. Kneipp, M. Moskovits, H. Kneipp eds.), p. 125-146, Springer-Verlag Berlin Heidelberg, 2006

[74] K Geetha*, Surface Enhanced Raman Scattering of Benzene Naphthalene and Anthracene Derivatives*, Mother Teresa Womens University, March, 2015 (Ph.D Thesis).

[75] J. Nedderson, G. Chumanov and T.M. Cotton, *Appl. Spectrosc*., **47** (1993) 1959.

[76] M. Vinod and K.G. Gopchandran, *Prog. Nat. Sci. Mater. Int*., **24** (2014) 569.

[77] N.D. Israelsen, C. Hansonand and E. Vargis, *Sci. World J*., **2015** (2015) 124582.

[78] R. Stiufiuc, C. Iacovita, C.M. Lucaciu, G. Stiufiuc, A.G. Dutu, C. Braescu and N. Leopold, *Nanoscale Res. Lett*., **8** (2013) 47.

[79] J.A. Creighton, C.G. Blatchford and M. G. Albrecht, *J. Chem. Sot. Faraday Trans. II* **75** (1979) 790.

[80] U.K. Sarkar, S. Chakrabarti and T.N. Misra, *J. Raman Spectrosc*., **16** (1993) 97.

[81] P.C. Lee and D. Meisel, *J. Phys. Chem*., **86** (1979) 790.

[82] S. Sanchez Cortes and J.V. Garcia Ramos, *Vib. Spectrosc*., **4** (1993) 185.

[83] G.A. López-Muñoz, J.A. Pescador-Rojas, J. Ortega-Lopez, J.S. Salazar and J.A. Balderas-López, *Nanoscale Res. Lett*., **7** (2012) 423.

[84] A. Khan, A. Rashid, R. Younas and R. Chong,, *Int. Nano. Lett.*, **6** (2016) 21.

[85] A.T. Shah, S. Ahmad, M.F. Khan, K. Shahzad, S. Tabassum and A. Mujahid, *Arabian. J. Chem*., **9** (2016) 537.

[86] S. Lambert, C. Cellier, E. M. Gaigneaux, J.P. Pirard and B. Heinrichs, *Catal. Commun.*, **8** (2007)1244.

[87] H. Zhang, Q. Zhu, Y. Zhang, Y. Wang, L. Zhao and B.Yu, *Adv. Funct. Mater*.,**17** (2007) 2766

[88] Z. Liu and Y. Bando, *Adv. Mater*.,**15** (2003) 303.

[89] J.R. Oritz, T. Ogura, J. Medina-Valtierra, S.E. Acosta-Ortiz, P. Bosh, J.A. De las Reyes and V.H. Lara, *Appl. Surf. Sci*., **174** (2001)177.

[90] A. Anzlovar, Z.C. Orel and M. Zigon, *Journal of the European Ceramic Society,* **27** (2007) 987.

[91] B. Wiley, Y. Sun, B. Mayers and Y. Xia, *Chem. Eur. J.*, **11** (2005) 454.

[92] F. Tian, F. Bonnier, A. Casey, A.E. Shanahan and H.J. Byrne, *Anal. Methods*, **6** (2014) 9116.

[93] J. Pulit, M. Banach and Z. Kowalski, CHEMIK, **65** (2011) 445.

[94] F. Benz, R. Chikkaraddy, A. Salmon, H. Ohadi, B. de Nijs, J. Mertens, C. Carnegie, R. W. Bowman and J. J. Baumberg, J. Phys.Chem. Lett., **7** 2016) 2264.

[95] D. Jimenez de Aberasturi, A. B. Serrano-Montes, J. Langer, M. Henriksen-Lacey, W. J. Parak and L. M. Liz-Marzán, Chem. Mater., **28** (2016) 6779.

[96] A. La Porta, A. Sánchez-Iglesias, T. Altantzis, S. Bals, M. Grzelczak and L. M. Liz-Marzán, Nanoscale, **7** (2015) 10377.

[97] A.X. Wang and X. Kong, *Materials,* **8** (2015) 3024.

[98] O. Alharbi, Y. Xu and R. Goodacre, *Analyst,* **139** (2014) 4820.

[99] S. Mabbott, O. Alharbi, K. Groves and R. Goodacre, *Analyst*, **140** (2015) 4399.

[100] O. Alharbi, Y. Xu and R. Goodacre, *Analyst*, **140** (2015) 5965.

[101] Y. Zhang, Z. Wang, L. Wu, Y. Pei, P. Chen and Y. Cui, *Analyst* , **139** (2014) 5148.

[102] C. Andreou, M.R. Hoonejani, M.R. Barmi, M. Moskovits and C.D. Meinhart, *ACS Nano*, **7** (2013) 7157.

[103] N.D. Kline, A. Tripathi, R. Mirsafavi, I. Pardoe, M. Moskovits, C. Meinhart, J.A. Guicheteau, S.D. Christesen, A.W. Fountain, *Anal. Chem*., **88** (2016) 10513.

[104] S. Yang, X. Dai, B.B. Stogin and T.S. Wong, *Proc. Natl. Acad. Sci. USA*, **113** (2016) 268.

[105] N.A. Hatab, G. Eres, P.B. Hatzinger and B. Gu, *J. Raman Spectrosc*., **41** (2010) 1131

[106] D. Zeisel, V. Deckert, R. Zenobi and T Vo Dinh, Chem. Phys. Lett., **283** (1998) 381.

[107] L.A. Dick, A.D. McFarl and, C.L. Haynes and R.P. van Duyne, *J. Phys. Chem. B*., **106** (2002) 853.

[108] J.A.S. Gil and J.V.G. Ramos, *J. Chem. Phys*., **108** (1998) 317.

[109] R.N.Dr. Natália Šmídová in: *Optimization of surface-enhanced Raman scattering spectroscopy for study of biologically important biomolecules and their interactions*, Institute of Physics of Charles University (32-FUUK), (Ph. D. Thesis).

[110] X. Dong, H. Gu, J. Kang, X. Yuan and J. Wu, *J. Mol. Struct*., **984** (2010) 396.

[111] G. Li and P. Miaoin: *Electrochemical Analysis of Proteins and Cells,* SpringerBriefs in Molecular Science, (Springer-Verlag Berlin Heidelberg, 2013) p 19.

[112] D.C. Johnson and W.R. Lacourse, *Anal. Chem*., **62** (1990) A589.

[113] B. Bas, M. Jakubowska and Z. Kowalski, *Electroanal*, **18** (2006) 1710.

[114] C.H. Fan, G.X. Li, Y. Zhuang, J.Q. Zhu and D. X. Zhu, *Electroanal*, **12** (2000) 205.

[115] A. Gutes, C. Carraro and R. Maboudian, *Electrochim Acta*, **56** (2011) 5855.

[116] G.X. Li, X.M. Liao, H.Q. Fang and H.Y. Chen, *J. Elect. Chem*., **369** (1994) 267

[117] G.X. Li, H.Y. Chen and D.X. Zhu, *c. Anal.Chim. Acta.*, **319** (1996) 275.

[118] M.J. Eddowes and H.A. O. Hill, *J Chem. Soc.Chem.Commun.,* **21** (1977) 771.

[119] L.A. Colon, R. Dadoo and R.N. Zare, *Anal. Chem*., **65** (1993) 476.

[120] S. Wasmus and A. Kuver. *J. Electroanal Chem.*, **461** (1999) 14.

[121] A. Axelevitch, B. Apter and G. Golan, *Opt. Express*, **21** (2013) 4126.

[122] J.E. Greene in: *Handbook of Deposition Technologies for Films and Coating*, 3rd Ed., Ed. P. M. Martin, ed. (Elsevier,) Chap. **12** (2010) 554.

[123] M. Meier, A. Wokaun and T.Vo Dinh, *J. Phys. Chem*., **89** (1985) 1843.

[124] T.V. Dinh, M. Meier and A. Wokaun, *Anal. Chim. Acta*., **181** (1986) 139.

[125] C. Jennings, R. Aroca, A.M. Hor and R.O. Loutfy, *Anal. Chem*., **56** (1984) 2033.

[126] R. Aroca and F. Martin, *J .Raman Spectrosc*., **17** (1986) 243.

[127] R.P. van Duyne, J.C. Hulteen and D.A. Treichel, *J. Chem. Phys*., **99** (1993) 2101.

[128] L.L. Hench and J.K. West, *Chem. Rev*., **90** (1990) 33.

[129] D. Avnir, *Acc. Chem. Res*., **28** (1995) 328.

[130] R. Gupta and N.K. Chaudhury, *Bios. Bioe*., **22** (2007) 2387.

[131] W.Y. Cai, Q. Xu, X.N. Zhao, J. H. Zhu and H.Y. Chen, *Chem. Mater*., **18** (2006) 279.

[132] X.H. Kang, J. Wang, Z.W. Tang, H. Wu and Y.H. Lin, *Talanta*., **78** (2009) 120.

[133] Y. Wang, Y. Wu, J. Wang and J. Di, *Bioprocess Biosyst. Eng.*, **32** (2009) 531.

[134] J. Z. Xu, Y. Zhang G. X. Li and J. J. Zhu, *Mat. Sci. Eng. C-Bio*. S, **24** (2004) 833.

[135] C.J. Zhong and M.D. Porter, *Anal. Chem*., **67** (1995) A709.

[136] D. Mandler and I. Turyan, *Electroanal*, **8** (1996) 207.

[137] C.J. Zhong and M.D. Porter, *Anal. Chem*., **67** (1995) A709.

[138] R. Otero, F. Rosei and F. Besenbacher,Annu. *Rev. Phys. Chem*., **57** (2006) 497.

[139] T.C. Tseng,C. Urban , Y. Wang, R. Otero, S.L. Tait, M. Alcami, D. Ecija, M. Trelka , J.M. Gallego, N. Lin, M. Konuma , U. Starke, A. Nefedov, A. Langner,C. Woll , M.A. Herranz, F. Martin , N. Martin, K. Kern and R. Miranda, *Nat. Chem*., **2** (2010) 374.

[140] L.L. Chua, J. Zaumseil, J.F. Chang, E.C. W. Ou, P.K.H. Ho, H. Sirringhaus and R.H. Friend, *Nature*, **434** (2005) 194.

[141] C.D. Dimitrakopoulos and P.R.L. Malenfant, *Adv. Mater*., **14** (2002) 99.

[142] H. Ishii, K. Sugiyama, E. Ito and K. Seki, *Adv. Mater*., **11** (1999) 605.

[143] X.G. Qu, J. Chou, T.H. Lu, S.J. Dong, C. L. Zhou and T.M. Cotton,, *J. Electroanal. Chem.,* **381** (1995) 81.

[144] H. Syed, G.K. Podagatlapalli, M.A. Mohiddon and V.R. Soma, *Adv. Mater. Lett*., **6** (2015) 1073.

[145] Y. Han, X. Lan, T. Wei, H.L. Tsai and H. Xiao, *Appl. Phys*., **97** (2009) 721.

[146] C.H. Lin, L. Jiang, Y.H. Chai, H. Xiao, S.J. Chen and H.L. Tsai, *Opt. Express*, **17** (2009) 21581.

[147] Z.Q. Zhu, Z.D. Yan, P. Zhan and Z.L. Wang, *Sci. China Phys. Mech. Astron*., **56** (2013) 1806.

[148] J. Yang, J. Li, Z. Du, Q. Gong, J. Teng and M. Hong, *Sci. Rep*., **4** (2014) 6657.

[149] J.C. Hulteen, D.A. Treichel, M.T. Smith, M.L. Duval, T.R. Jensen and R.P. van Duyne, *J. Phys. Chem*., **103** (1999) 3854.

[150] C.L. Haynes and R.P. van Duyne, *J. Phys. Chem., B*, **105** (2001) 5599.

[151] S. Mahajan, M. Abdelsalam, Y. Suguwara, S. Cintra, A. Russell, J. Baumberg and P. Bartlett, *Phys. Chem. Chem. Phys*., **9** (2007) 104.

[152] P.L. Stiles, J.A. Dieringer, N.C. Shah and R.P. van Duyne, *Annu. Rev. Anal. Chem*., **1** (2008) 601.

[153] J.F. Bryche, A. Tsigara, B. Bélier, M.L.M. de la Chapelle, M.T.G. Canva, B. Bartenlian and G. Barbillon, *Sens. Actuators*, **2228** (2016) 31.

[154] M. Jahn, S. Patze, I.J. Hidi, R. Knipper, A.I. Radu, A. Mühlig, S. Yüksel, V. Peksa, K. Weber and T. Mayerhöfer, et al., *Analyst*, **141** (2016) 756.

[155] D.Y. Wu, J.F. Li, B Ren and Z.Q. Tian, *Chem. Soc. Rev*., **37** (2008) 1025.

[156] N. A. Abu Hatab, J. M. Oran and M. J. Sepaniak, *ACS. Nano.*, **2**, (2008) 377.

[157] L. Petti, R. Capasso, M. Rippa, M. Pannico, P. La Manna, G. Peluso, A. Calarco, E. Bobeico and P.A. Musto, *Vib. Spectrosc*., **82** (2016) 22.

[158] N.A. Cinel, S. Cakmakyapan, S. Butun, G. Ertas and E. Ozbay, *Photonics Nanostruct. Fundam. Appl*., **15** (2015) 109.

[159] W. Yue, Z. Wang, Y. Yang, L. Chen, A. Syed, K. Wong and X. Wang, *J. Micromech. Microeng.,* **22** (2012) 125007.

[160] B.D. Gates, Q. Xu, M. Stewart, D. Ryan, C.G. Willson and G.M. Whitesides, *Chem. Rev.*, **105** (2005) 1171.

[161] M. Altissimo, *Biomicrofluidics*, **4,** (2010) 3.

[162] Real-Time Analyzers. Available online: http://rta.biz/products/sers-products/ (*accessed on 2 June 2017*).

[163] Sigma-Aldrich. Gold Nanoparticles, 10 nm Diameter, Silica Coated, Dispersion inWater. Available online: http://www.sigmaaldrich.com/catalog/product/aldrich/747564?lang=en&region=US *(accessed on 2 June 2017*).

[164] Sigma-Aldrich. Gold Nanorods, 10 nm Diameter, Silica Coated, Dispersion in Water. Available online: http://www.sigmaaldrich.com/catalog/product/aldrich/747998?lang=en&region=US *(accessed on 2 June 2017*).

[165] Horiba Scientific. Available online: http://www.horiba.com/us/en/scientific/products/raman-spectroscopy/accessories/sers-substrates/ (*accessed on 2 June 2017*).

[166] Ocean Optics. Available online: https://oceanoptics.com/product/sers/ (accessed on 2 June 2017).

[167] AtoID. Available online: http://www.atoid.com/shop/ (*accessed on 2 June 2017*).

[168] E. Rinnert in: *Handbook of Enhanced Spectroscopy*; P.G. Gucciardi, M.L. de la Chapelle, N. Lidgi-Guigui, and C.R.C. Eds., Press: Boca Raton, FL, USA, (2015) 342.

[169] Silmeco. Available online: http://www.silmeco.com/products/sers-substrate-serstrate/ *(accessed on 2 June 2017).*

[170] P. Owens, N. Phillipson, J. Perumal G.M. O'Connoer and M. Olivo, *Biosensors*, **5** (2015) 664.

[171] Mesophotonics. Available online: http://www.mesophotonics.com/sers_central/index.html (accessed on 2 June 2017).

[172] K. Faulds, A. Hernandez-Santana, and W.E. Smith in: *Spectroscopic Properties of Inorganic and Organometallic Compounds: Techniques, Materials and Applications*; J. Yarwood, R. Douthwaite and S.Duckett, , Eds.; Royal Society of Chemistry: London, UK, 2010; pp. 1–21.

[173] Diagnostic anSERS Inc.: Available online: https://www.diagnosticansers.com/ (*accessed on 2 June 2017*).

[174] W.W. Yu and I.M. White, *Anal. Chem*., **82** (2010) 9626.

[175] W.W. Yu and I.M. White, *Analyst*, **137** (2012) 1168.

[176] E.P. Hoppmann, W.W. Yu and I.M. White, *Methods*, **63** (2013) 219.

[177] W.W. Yu and I.M. White, *Analyst,* **138** (2013) 1020.

[178] H.W. Schroetter and H.W. Kloeckner, in: *Raman Spectroscopy of Gases and Liquids.* Weber A. (eds), *Topics in Current Physics,* **vol 11**. Springer Berlin Heidelberg, 1979.

[179] M. Moskovits, *J. Raman Spectrosc*., **36** (2005) 485.

[180] H. Xu, J. Aizpurua, M. Käll and P. Apell, *Phys. Rev. E*, **62** (2000) 4318.

[181] E. Le Ru and P. Etchego in:, *Principles of Surface-Enhanced Raman Spectroscopy and Related Plasmonic Effects* (Elsevier, Oxford, UK, 2009).

[182] A. Otto in:, *"Classical" and "Chemical" Origins, in Light Scattering in Solids IV, Eds. M. Cardona and G. Güntherodt, Topics in Applied Physics* (Springer-Verlag, Berlin, 1984)

[183] W.L. Barnes, A. Dereux and T.W. Ebbesen, *Nature*, **424** (2003) 824.

[184] L, Yajing, *Surface Enhanced Vibrational Spectroscopy and Electrical Characterization On Nanojunctions*, Rice University, June, 2016 (Ph.D. Thesis).

[185] H. Raether in: *Surface Plasmons on Smooth and Rough Surfaces and on Gratings,* Springer (1988).

[186] B.W.Ninham, C.J. Powell and N. Swanson, *Phys. Rev.,* **145** (1966) 209.

[187] C. Sönnichsen,et al., *Phys. Rev. Let,*.**88** (2002) 77402.

[188] K.C. Lee, S. J. Lin, C.H. Lin, C.S. Tsai and Y.J. Lu, *Surface and Coatings Technology,* **202** (2008)5339.

[189] S.Peng, J.M. McMahon, G.C. Schatz, S.K. Gray and Y.Sun, *PNAS.,* **107** (2010) 14530.

[190] S.Link and M.A. El-Sayed, *International Reviews in Physical Chemistry,* **19** (2000) 409.

[191] H.Wang, D.W. Brandl, F. Le, P. Nordlander and N.J. Halas, *Nano Lett.,* **6** (2006) 827.

[192] J.A. Fan et al., *Science,* **328** (2010) **112.**

[193] S.L.Westcott, S.J. Oldenburg, T.R. Lee and N.J. Halas, *Langmuir,* **14** (1998) 5396.

[194] G.V. Naik, V.M. Shalaev and A. Boltasseva, *Adv. Mater.,* **25** (2013) 3264.

[195] N.K. Grady, N.J. Halas and P.Nordlander, *Chem.Phy. Lett.,* **399** (2004) 167.

[196] T.Holmgaard and S.I. Bozhevolnyi, *Phys. Rev. B,* **75** (2007) 245405.

[197] Wiley: Introduction to Solid State Physics, 8th Edition - Charles Kittel. Available at: http://www.wiley.com/WileyCDA/WileyTitle/productCd-EHEP000803.html. (*accessed: 27th May 2016*)

[198] T. Holmgaard and S. I. Bozhevolnyi, *Phys. Rev., B,* **75** (2007) 245405.

[199] S. L.Westcott, S. J.Oldenburg, T. R.Lee and N. J. Halas, *Langmuir,* **14** (1998) 5396.

[200] K Hasna in: *Development of metal and metal oxide nanostructures for Surface Enhanced Raman Scattering*, Department of Instrumentation Cochin University of Science and Technology, Cochin - 682022, Kerala, India, August, 2016 (Ph. D. Thesis).

[201] J.M. Brockman, B.P. Nelson and R.M. Corn, *Annu. Rev. Phys. Chem*., **51** (2000) 41.

[202] W. Knoll, *Annu. Rev. Phys. Chem*., **49** (1998) 569.

[203] K.L. Kelly, E. Coronado, L.L. Zhao and G.C. Schatz, *J. Phys. Chem*. *B*, **107** (2003) 668.

[204] A.J. Haes, C.L. Haynes, A.D. McFarland, G.C. Schatz, R.P. Van Duyne and S. Zou, *MRS Bull.,* **30** (2011) 368.

[205] O.Benson, *Nature,* **480** (2011)193.

[206] M.A. Garcia, *J. Phys. D. Appl. Phys*., **44** (2011) 283001.

[207] Li, Yajing in: *Surface Enhanced Vibrational Spectroscopy and Electrical Characterization on Nanojunctions* (2016) Diss., Rice University. http://hdl.handle.net/1911/95583.

[208] K.L. Kelly, E. Coronado and L. Zhao, G.C. Schatz, *J. Phys. Chem.,* **B 107 (**2003) 668.

[209] G.C.Schatz and R.P.Van Duyne, In: *Handbook of Vibrational Spectroscopy*, J.M. Chalmers and P.R. Griffiths (Eds), John Wiley & Sons Ltd, Chichester, 2002 pp 759

[210] G.Mie, *Ann. Phys.,* **330 (**1908) 377.

[211] C.R. Bohren and D.F. Huffman in: *Absorption and Scattering of Light by Small Particles.* Wiley Interscience, New York (1983).

[212] S. Link and M.A. El-Sayed,.*J. Phys. Chem. B,* **103** (1999) 8410.

[213] M.D.Malinsky, K.L.Kelly, G.C.Schatz and R.P. Van Duyne , *J. Phys. Chem. B***, 105,** (2001) 2343.

[214] R.L. McCreery in: *Raman Spectroscopy for Chemical Analysis,* Wiley Interscience, 2000.

[215] M.Kerker, D.S.Wang and H. Chew, *Appl. Opt.,* **19 (**1980) 3373.

[216] D.S.Wang and M.Kerker,.*Phys. Rev. B,* **24** (1981) 1777.

[217] A.D. McFarland, M.A. Young, J.A. Dieringer and R.P. van Duyne., *J. Phys. Chem. B***, 109 (**2005**)** 11279.

[218] R. Aroca in: *Surface-Enhanced Vibrational Spectroscopy,* (John Wiley & Sons, Ltd, Chichester, UK, 2006).

[219] G. Sun in: *Surface-Enhanced Raman Spectroscopy Investigation of Surfaces and Interfaces in Thin Films on Metals*, Ruhr University Bochum, China, 2007 (Ph. D. Thesis).

[220] J. R. Lambardi, R. L. Birke, T. Lu and J. Xu, *J. Chem. Phys*., **84** (1986) 4174.

[221] S. Guoguangin: *Surface-enhanced Raman Spectroscopy Investigation of Surfaces and Interfaces in Thin Films on Metals*, Faculty of Mechanical Engineering the Ruhr-University Bochum, Bochum (2007) (Ph.D. Thesis)

[222] (a) Z. Q. Tian and B. Ren, *Wiley & VCH*, **3** (2003), p575.

(b) Tuan Vo-Dinh, *Trends in Anal. Chem.,* **17** (1998) 558.

[223] H. Kneipp, I. Itzkon, R.R. Dasar and M.S. Feld, *Chem. Rev*., **99** (1999) 2957.

[224] M. Volkan, D.L. Stokes and T. Vo Dinh, *J. Raman Spectrosc*., **30** (1999) 1057.

[225] M.Y. Sha, H. Xu, S.G. Penn and R. Cromer, *Nanomed,* **2** (2007) 725.

[226] C.C. Lin, Y.M. Yang, Y.F. Chen, T.S. Yang and H.C. Chang, *Biosens Bioelectron,* **24** (2008) 178.

[227] X.M. Qian and S.M. Nie, *Chem Soc Rev*, **37** (2008) 912.

[228] N. Weissenbacher, B. Lendl, J. Frank, H.D.Wanzenboeck, B. Mizaikoff and R.J Kellner, *Mol. Struct.,* **410-411** (1997) 539.

[229] C.J. McHugh, R. Keir, D. Graham and W.E. Smith, *Chem. Commun*., **21** (2002)580.

[230] J.M. Sylvia, J.A. Janni, J.D. Klein and K.M Spencer, *Anal. Chem*., **72** (2000) 5834.

[231] N. Taranenko, J.P. Alarie, D.L. Stokes and T. Vo-Dinh, *J. Raman Spec*., **27** (1996) 379.

[232] T. Vo Dinh, D.L. Stokes, G.D. Griffin, M. Volkan, U.J. Kim and M.I. Simon, *J. Raman Spec.*, **30** (1999) 785.

[233] A. Loren, C. Eliasson, M. Josefson, K. Murty, M. Kall, J. Abrahamsson and K. Abrahamsson, *J. Raman Spec.*, **32** (2001) 971.

[234] R. Sulk, C. Chan, J. Guicheteau, C. Gomez, J.B.B. Heyns, R. Corcoran, K. Carron, *J. Raman Spec.*, **30** (1999) 853.

[235] E. Kammer, K. Olschewski, S. Stockel, P. Rosch, K. Weber, D. Cialla-May, T. Bocklitz, and J. Popp, *Anal. Bioanal. Chem.,* **407** (2015) 8925.

[236] W. Shen, X. Lin, C. Jiang, C. Li, H. Lin, J. Huang, S. Wang, G. Liu, X. Yan, Q. Zhong, and B. Ren, *Angew. Chem. Int. Ed.,* **54** (2015) 7308.

[237] [230] H.Y. Chen, M.H. Lin, C.Y. Wang, Y.M. Chang, and S. Gwo, *J. Am. Chem. Soc.,* **137** (2015)13698.

[238] M.F. Kircher, A. de la Zerda, J.V. Jokerst, C.L. Zavaleta, P.J. Kempen, E. Mittra, K. Pitter, R. Huang, C. Campos, F. Habte, R. Sinclair, C.W. Brennan, I.K. Mellinghoff, E.C. Holland, and S.S. Gambhir, *Nature Med.,* **18** (2012) 829.

[239] B.N.V. Kumar, S. Guo, T. Bocklitz, P. Rosch, and J. Popp, *Anal. Chem.,* **88** (2016) 7574.

[240] A. Walter, A. Marz, W. Schumacher, P. Rosch, and J. Popp, *Lab on Chip,* **11** (2011) 1013.

[241] M.J. Kale, T. Avanesian, and P. Christopher, *ACS Catal.,* **4** (2013) 116.

[242] L. Zhou, C. Zhang, M.J. McClain, A. Manjavacas, C.M. Krauter, S. Tian, F. Berg, H.O. Everitt, E.A. Carter, P. Nordlander, and J.J. Halas, *Nano Lett.,* **16** (2016) 1478.

[243] S. Schlücker, *Angew. Chem. Int. Ed*., **53** (2014) 4756.

[244] H. Kim, K. M. Kosuda, R. P. Van Duyne and P. C. Stair, *Chem. Soc. Rev*., **39** (2010) 4820.

[245] Z.Q. Tian and B. Ren, *Annu. Rev. Phys. Chem.*, **55** (2004) 197.

[246] B. Ren, Y. Cui, D.Y. Wu and Z.Q. Tian in: *Surface Enhanced Raman Spectroscopy* (Ed.: S. Schlcker), Wiley-VCH, Weinheim, 2011, pp. 191 – 218.

[247] X. Li and A. A. Gewirth, *J. Am. Chem. Soc.,* **127** (2005) 5252.

[248] A. Wang, Y. F. Huang, U. K. Sur, D. Y. Wu, B. Ren, S. Rondinini, C. Amatore and Z. Q. Tian, *J. Am. Chem. Soc.,* **132** (2010) 9534.

[249] W. Xie, C. Herrmann, K. Kçmpe, M. Haase and S. Schlcker, *J. Am. Chem. Soc.,* **133** (2011) 19302.

[250] A. Kranich, H. K. Ly, P. Hildebrandt and D. H. Murgida, *J. Am. Chem. Soc.,* **130** (2008) 9844.

[251] D. H. Murgida and P. Hildebrandt, *Chem. Soc. Rev.,* **37** (2008) 937.

[252] H. K. Ly, M. Sezer, N. Wisitruangsakul, J. J. Feng, A. Kranich, D. Millo, I. M. Weidinger, I. Zebger, D. H. Murgida and P. Hildebrandt, *FEBS J.,* **278** (2011) 1382.

[253] P. Hildebrandt, J.J. Feng, A. Kranich, K.H. Ly, D.F. Martn, M. Mart, D.H. Murgida, D.A. Paggi, N. Wisitruangsakul, M. Sezer, I. M. Weidinger and I. Zebger

in: *Surface Enhanced Raman Spectroscopy* (Ed.: S. Schlcker), Wiley-VCH, Weinheim, 2011, pp. 219 – 240.

[254] M.D. Barnes, W.B. Whitten and J. M. Ramsey, *Anal. Chem*., **418A** (1995) 67

[255] R. Keller *et al., Los Alamos Annual Report*, 1990, p. 55.

[256] S. Nie and S.R. Emory, *Science*, **275** (1997) 1102.

[257] K. Kneipp, Y. Wang, H. Kneipp, L. T. Perelman, I. Itzkan, R. R. Dasari and M.S. Feld, *Phys. Rev. Lett*., **78** (1997) 1667

[258] E.C. Le Ru, M. Meyer and P.G. Etchegoin, *J. Phys. Chem. B,* **110** (2006) 1944.

[259] J.A. Dieringer, R.B. Lettan II, K.A. Scheidt and R. P. Van Duyne, *J. Am. Chem. Soc.,* **129** (2007) 16249.

[260] K. E. Shafer-Peltier, C. L. Haynes, M. R. Glucksberg and R. P. Van Duyne, *J. Am. Chem. Soc.*, **125** (2003) 588.

[261] R.J. McNichols and G.L.J. Cote, *Biomed. Opt*., **5** (2000) 5.

[262] P.G. Steffes, *Diabetes Technol. Ther*., **1** (1999) 129

[263] P. Freunscht, R.P. Van Duyne and S.Schneider, *Chem. Phys. Lett.*, **281** (1997) 372.

[264] T.O. Deschaines and K.T. Carron, *Appl. Spectrosc.*, **51** (1997) 1355.

[265] D.B. Gomis, J.M. Tamayo and J.M. Alonso, *Anal. Chim. Acta*, **436** (2001) 173.

[266] L.Yang, E. Janle, T. Huang, J. Gitzen, P.T. Kissinger, M. Vreeke and A. Heller, *Anal. Chem.*, **34** (1995) 1326.

[267] K.T. Carron and B.J. Kennedy, *Anal. Chem.*, **67** (1995) 3353.

[268] M.M. Walczak, C. Chung, S.M. Stole, C.A. Widrig and M.D. Porter, *J. Am. Chem. Soc*., **113** (1991) 2370

[269] H.T. Eastment and W.J. Krzanowski, *Technometrics*, **24** (1982) 73.

[270] E.B. Martin and A.J. Morris, *Annu. Rev. Control*, **23** (1999) 35.

[271] A. Ho¨skuldsson, *J. Chemom*., **29** (1988) 409.

[272] R.Ravanshad, A.K. Zadeh, A.M. Amani, S.M.Mousavi, S.A. Hashemi, A.S.Dashtaki, E. Mirzaei and B. Zare, *Nano Reviews & Experiments*, **9** (2018)1

[273] C. Kallaway, L.M. Almond, H, Barr, J. Wood, J. Hutchings, C. Kendal and N. Stone, *Photodiagnosis Photodyn Ther.,* **10** (20133) 207.

[274] H. Abramczyk and B. Brozek-Pluska, *Chem Rev.*, **113** (2013) 5766.

[275] J.C. Day, R. Bennett, B, Smith, C. Kendall, J. Hutchings, G.M. Meaden, et al., *Physics in Medicine and Biology*, **54** (2009) 7077.

[276] WHO Iafroc in: *GLOBOCAN, graph production: Global Cancer Observatory. Estimated number of incident cases of top 10 cancers. CA: A Cancer Journal for Clinicians;* 2012.

[277] J.Yan Yang, J. Walicki, A. Abderrahmani, M. Cornu, G. Waeber, B. Thorens and C. Widmann, The J. Biol. Chem., **280** (2005) 32835.

[278] J. Yang, Z. Wang, S. Zong, C. Song , R. Zhang and Y Cui, *Anal Bioanal Chem.,* **402** (2012) 1093.

[279] H. Li, D. Hasan, R.S. Ruoff, et al., *Advanced Functional Materials.,* **23** (2013) 4332.

[280] U.S. Dinish, F.C. Yaw, A. Agarwal and M. Olivo, *Bioelectron.*, **26** (2011) 1987.

[281] X. Wang, X. Qian, J.J. Beitler , Z.G. Chen, F.R. Khuri, M.M. Lewis, H.J. Shin, S. Nie and D.M. Shin, *Cancer Res*., **71** (2011) 1526.

[282] L. Beqa, Z. Fan, A.K. Singh, D. Senapati and P.C. Ray, *ACS Appl Mater Interfaces.,* **3** (2011) 3316.

[283] M.C. da Paz, M. de Fátima, M.A. Santos, C.M.B. Santos, S.W. da Silva, L.B. de Souza, E.C.D. Lima, R.C. Silva, C.M. Lucci, P.C. Morais, R.B. Azevedo and Z.G.M. Lacava, *Int J Nanomed.*, 7 (2012) 5271.

[284] D. Aydin, M. Feychting and J. Schüz, *J Natl Cancer Inst.,* **103** (2011) 1264.

[285] M.F. Kircher, A. de la Zerda, J.V. Jokerst, C.L. Zavaleta,. P.J. Kempen, E. Mittra, K. Pitter, R. Huang, C. Campos, F. Habte, R. Sinclair, C.W. Brennan, I. K. Mellinghoff, E.C. Holland and S.S. Gambhir, *Nat Med.,* **18** (2012) 829.

[286] F. Zheng, Y. Qin and K. Chen, *J Biomed Opt.*, **12** (2007) 034002.

[287] L. Zhao, T.H. Kim, H.W. Kim, J.C. Ahn and S.Y. Kim, *Acta Biomater.*, **20** (2015) 155.